Efficient genetic code expansion tools enable *in vivo* study of lysine acetylation in non-model bacteria

Elise Van Fossen[1]*, Molly Stephenson[1], Andrew Frank[1], Soujanya Akella[1], Rowan Wooldridge[1], Andrew Wilson[1], Youngki You[1], Ernesto Nakayasu[1], Rob Egbert[1], Joshua Elmore[1]*

[1]Biological Sciences Division, Pacific Northwest National Laboratory, Richland, WA USA

*Correspondence should be addressed to Elise Van Fossen (elise.vanfossen@pnnl.gov) and Joshua Elmore (joshua.elmore@pnnl.gov)

ABSTRACT

Recent proteomic advancements have revealed widespread Nε-lysine acetylation in pathways governing pathogenicity, metabolism, and antibiotic resistance in bacteria. The spontaneous, non-specific nature of this modification in prokaryotes obscures its biological role, necessitating prokaryotic specific *in vivo* interrogation systems. Genetic Code Expansion (GCE) offers a powerful method to investigate the roles and regulation dynamics of acetyl-lysine *in vivo* with the precise incorporation of a suite of non-canonical amino acids, including acetyl-lysine analogs. However, its use has been largely restricted to *Escherichia coli* strains due to challenges associated with implementation and optimization of the technology in more diverse bacterial strains. Here, we present a bacterial host-agnostic, readily optimizable genetic code expansion platform designed to site-specifically incorporate non-canonical amino acids (ncAAs) into target proteins within living bacteria. We further demonstrate the versatility of this technology by showcasing, for the first time, the successful incorporation of acetyl-lysine in a non-*E. coli* bacterium.

INTRODUCTION

Over the past decade, it has become apparent that PTMs play crucial physiological roles in microbial organisms[1, 2]. The establishment of a comprehensive biological framework that encompasses the characteristics, regulatory mechanisms, and functions of bacterial PTMs, will unveil new opportunities for bioengineering and the treatment of infectious diseases[2]. Yet, PTMs remain one of the largest black boxes in our understanding of bacterial physiology[1-4].

Nε-lysine acetylation is one such modification that has recently emerged as a potentially significant player in bacterial physionlogy[5-7]. Once considered rare in bacteria, advances in proteomic analysis have now enabled high-sensitivity analyses of bacterial proteomes, revealing extensive lysine acetylation (up to 40% of all bacterial proteins) in more than 30 different bacterial species[8-11]. Proteomic[5, 10, 12-15] and *in vitro* studies[5, 16-21] have connected lysine acetylation to key metabolic and regulatory functions, including the regulation of central metabolism[5, 6, 22], transcription[6, 7, 23] and translation[24] as well as modulating pathogeneticity[25] and antibiotic resistance[26]. The pervasive presence of acetyl-lysine in these systems indicate that microbial bioengineering efforts and antibacterial designs that are naïve to endogenous acetylation mechanisms may exhibit diminished efficiency and efficacy upon implementation. Further, the systems that govern acetylation themselves are likely to be powerful targets for engineering enhancement and therapeutic intervention.

Our understanding of lysine acetylation in bacterial systems remains limited due to several complicating factors. Firstly, lysine acetylation systems in bacteria differ greatly from eukaryotic systems and even vary widely among bacterial species, making it difficult to create generalized models for PTM mechaniscs[2, 7]. Secondly, lysine acetylation occurs at very low levels on numerous proteins and often in response to specific environmental conditions that can be challenging to consistently produce in model strains in typical laboratory conditions[6]. Additionally, because a significant proportion of lysine acetylation in bacteria occurs non-enzymatically and bacterial acetylases themselves are promiscuous, specialized biochemical tools are required to create acetyl lysine mimics for analysis[7, 8]. As a result, little is known about acetyl lysine regulatory mechanisms and interaction systems outside of *E. coli* and what is known in *E coli* may not translate to other bacteria.

Consequently, identifying the functional roles of lysine acylation and pinpointing the mechanisms that drive it is among the main challenges in bacterial biochemistry today. Doing so depends on the establishment two key capabilities: 1) to model the presence/absence of the PTM on a target protein, and 2) to reliably characterize the interacting entities or phenotypic fluctuations associated with each state[27]. Historically, most acetylation studies have used site-directed mutagenesis to substitute the lysine residue of interest with glutamine or arginine. These substitutions mimic acetyl-lysine and non-acetylated lysine, respectively[27]. While these studies have formed the basis of our understanding of lysine acetylation, this method has severe limitations as the substitutions replicate the electrostatic properties of the modifications but not their steric attributes. Consequently, there are numerous instances where this mutation does not accurately recapitulate the functional effects of acetyl-lysine[28, 29].

Advancements in synthetic and chemical biology have provided new technologies with which to augment lysine interrogation toolkits. Genetic code expansion (GCE) is one such technology, wherein engineered organisms can incorporate non-canonical amino acids (ncAAs), including PTM mimics, site-specifically into proteins, allowing the precise recapitulation of lysine

acetylation *in vivo* without relying on enzymatic action or site-directed mutagenesis. GCE technology has also provided ncAAs with unobtrusive crosslinking functionalities that facilitate the enrichment of and identification of PTM-driven protein-protein interactions.

As the induction of acetyl lysine occurs under specific environmental conditions that are challenging to replicate *in vivo*, functional investigations should take place directly in the strain of interest to achieve a more accurate and biologically relevant understanding[7, 23, 30]. *In vivo* application of GCE in bacteria is still nascent, but has already been impactful. In *Salmonella typhimurium*, genetically encoded incorporation of a non-hydrolysable BuK analogue into HilA demonstrated the consequences of specific butyrylation on infectivity[30] and, very recently, *in vivo* GCE was employed in *E. coli* to determine how acetylation modulates transcription factor DNA binding[23].

These two examples highlight the significant potential that *in vivo* genetic code expansion could offer for advancing our understanding of bacterial biology, though the technology still faces a critical limitation; the majority of development and optimization of GCE has been performed in laboratory strains of *E. coli*. As a result, as evidenced above, any *in vivo* implementation is typically constrained to *E. coli* or very similar species, and when working with more diverse bacteria, the efficacy of GCE elements must be determined through trial and error. Currently, there are few, if any, universal methods for optimizing GCE in non-*E. coli* strains. This limitation disproportionately impacts systems aimed at incorporating non-canonical amino acids with more subtle modifications, such as acetyl lysine. Incorporation efficiency for these smaller modifications tends to be lower compared to bulkier groups[31]. Consequently, optimizing these systems to perform robust science in non-model bacterial hosts remain technically challenging and laborious.

The lack of high-throughput genetic tools for the rapid optimization of expression levels of GCE machinery is a major bottleneck in applying GCE to non-model microbes. Common methods for transferring heterologous DNA into non-model bacteria—replicating plasmids, homologous recombination-based allelic exchange, and transposon mutagenesis—have limitations that restrict their utility. Replicating plasmids are often unstable, impose a fitness cost, and have a limited number of compatible plasmid options. While stable integration of heterologous DNA via transposon-based and homologous recombination-based technologies can bypass some of these problems, these methods are not suitable for high-throughput genetic engineering. Transposon-based tools have unpredictable integration sites, risking overestimation of GCE efficiency due to the influence of local environment on machinery expression. Homologous recombination, being low-efficiency and labor-intensive, is unsuitable for high-throughput assessments of translational machinery expression variants.

However, the genetic engineering platform SAGE (Serine recombinase-assisted genome engineering) and similar phase recombinase-based systems offer the potential to overcome these limitations by combing the high efficiency transformation of replicating plasmids, with the site specificity and stability of homologous recombination. SAGE is a highly efficient, and extensible technology that enables site-specific genome integration of multiple DNA constructs, often with efficiency on par with or superior to replicating plasmids[32]. The toolkit leverages high-efficiency serine recombinases, each transiently expressed from a non-replicating plasmid, to facilitate efficient, iterative integration of constructs or libraries into diverse bacterial genomes at unique attB sites. By utilizing non-replicating plasmids, SAGE is theoretically usable in any bacterial species and has been demonstrated in eight taxonomically-distinct bacteria thus far. As such, in this study we apply SAGE to implement and optimize genetic code expansion (GCE) in an

exemplar non-model organism, *Pseudomonas putida* KT2440, to demonstrate a generalizable workflow for onboarding genetic code expansion in organisms that are unrelated to *E. coli*. Leveraging these tools, we dramatically enhanced the efficiency of acetyl lysine incorporation—from nearly negligible levels to a robust system capable of encoding acetyl lysine at two distinct sites within a biologically relevant protein.

RESULTS

Multiplexed SAGE enables facile application of genetic code expansion in Pseudomonas putida KT2440

Plasmid-free genetic code expansion implementation requires the integration of an orthogonal translation system composed of, at minimum, three genetic elements into the chromosome of the host organism. These components include the orthogonal aminoacyl tRNA synthetase (o-aaRS), its cognate orthogonal tRNA (o-tRNA) and a target protein containing a 'blank' codon, typically a stop codon, at the site of ncAA incorporation[33].

Incorporating components separately provides the ability to independently test variants of each component. For this, we utilized a variation of serine recombinase-assisted genome engineering (SAGE) to incorporate multiple distinct 'target plasmids' into the chromosome without the need to excise the antibiotic selection marker between each incorporation (Figure 1C) as is required with the original SAGE implementation. For this, each component is linked with one of three antibiotic selection and serine recombinase combinations, which enables incorporation of each element into the chromosome in any order.

We decided to pursue the incorporation of the ncAA *para*-azido-L-phenylalanine (pAzF) with the *M. jannaschii* tyrosyl-tRNA synthetase/$tRNA^{Tyr}$ (*Mj*TyrRS/$tRNA^{Tyr}$) system, specifically the *para*-cyano-L-phenylalanine aminoacyl-tRNA synthetase (*p*CNF-RS) variant, for developing a SAGE-based genetic code expansion platform[34]. This system is a standard for GCE implementation in bacterial systems, as it is highly efficient and polyspecific with the ability to recognize at least 18 ncAAs, including *p*AzF, *p*CNF, and other *para* substituted phenylalanine analogues[34]. Additionally, pAzF is a valuable ncAA to encode as it contains a chemical handle compatible with crosslinking experiments, applicable for the identification of PTM interactions[35].

To develop a SAGE-based GCE system, we independently designed target plasmids containing each of the three required genetic elements (Figure 2A.) These plasmids also included distinct *attP* attachment sites for integration into three distinct *attB* sites in the bacterial chromosome by a set of three serine recombinases. Specifically, the *Mj*TyrRS element was designed for insertion at the TG1 *attB* site, the $tRNA^{Tyr}$ element at the BxB1 *attB* site, and the protein of interest, sfGFP in this case, at the R4 *attB* site. Non-replicating cargo plasmids were engineered with different antibiotic resistance markers to facilitate initial selection. However, once successful genetic integration was confirmed, maintaining antibiotic selection was unnecessary.

Our initial test platform for the SAGE-based GCE system was the bacterium *Pseudomonas putida* KT2440[36, 37]. KT2440 has become increasingly popular for industrial and environmental applications[38] due to its robust redox metabolism, high tolerance to diverse physicochemical stresses, rapid growth, versatile metabolism, and nonpathogenic nature. Recently, successful replicating plasmid-based GCE was reported in KT2440 for the first time[39] encouraging our efforts to use this system as a test-bed for our SAGE-based GCE system. For this, we used a SAGE-compatible strain of *P. putida* KT2440 called AG5577 for the basis of all further GCE development

and application in *P. putida*. This strain contains a collection of 9 distinct heterologous *attB* sequences that are each recognized by a distinct serine recombinase from the SAGE toolkit[32].

Multiple studies focused on implementing GCE in non-*E. coli* strains have reported that it is critical to adjust the regulatory elements (promoters, ribosome binding sites, etc.) for each new organism[40-42]. To maintain GCE components at physiologically relevant expression levels in *P. putida*, we followed a previously reported strategy[39, 42] wherein the most abundant codon in the KT2440 genome was identified (CUG, encoding leucine (Leu)) along with the associated aaRS and tRNA. Native promoters and terminators flanking $tRNA^{Leu}$ and leucyl-RS (LeuRS) were then used to control transcription of the *Mj* $tRNA^{Tyr}$ and *Mj*TyrRS, respectively.

Once all SAGE-GCE components were successfully ported into *P. putida*, the system efficiency was evaluated using a stop codon readthrough assay with sfGFP as a reporter. In this assay, we utilized an sfGFP variant with an amber mutation at the N150 codon ($sfGFP_{TAG150}$). In the absence of ncAA incorporation, expression of this reporter will lead to synthesis of a truncated, non-fluorescent, sfGFP protein. If the ncAA is incorporated into the protein at the amber codon (referred to as "suppression") a full length fluorescent sfGFP protein will be synthesized. The relative cellular fluorescence is directly correlated with production of ncAA-containing sfGFP protein. Consistent with what was previously reported in KT2440, we observed that the pCNF-RS system enabled efficient incorporation of pAzF as indicated by moderate expression of full-length sfGFP only in the presence of the ncAA (Figure 2B). Further top-down protein mass spectrometry (MS) analysis of the full-length purified protein confirmed the incorporation of pAzF (Figure S1).

Although this initial GCE system exhibited successful incorporation of pAzF, the efficiency could much improved. As a high concentration of orthogonal $tRNA^{CUA}$ is required for optimal incorporation efficiency in other GCE systems[43], we hypothesized that increasing the copy number of $tRNA^{CUA}$ could improve incorporation efficiency. To test this hypothesis, we designed our cassette to mimic an endogenous KT2440 tRNA operon, which encodes two identical $tRNA^{Leu}$ in a single pre-tRNA transcript (Figure 2A, GCE v2.0). This cassette incorporates the endogenous $tRNA^{Leu}$ promoter, the spacer sequence between the tRNAs, and the native downstream terminators, but replaces each $tRNA^{Leu}$ with a *Mj*$tRNA^{Tyr}$.

We also observed a KT2440 tRNA operon containing three tRNAs positioned upstream of a gene encoding an elongation factor protein (EF-Tu), an enzyme responsible for facilitating the transfer of aminoacyl-tRNA to the ribosome. As native EF-Tus can exhibit decreased efficiencies when operating in conjunction with ncAAs and orthogonal elements, we drew inspiration from the endogenous KT2440 operon and added an engineered EF-Tu—designed specifically for the incorporation of pAzF[44]—downstream of the dual *Mj*$tRNA^{Tyr}$ operon described above, creating GCE v2.5.

We further streamlined GCE v1.0 by combining the $sfGFP_{TAG150}$ reporter and *Mj*TyrRS on a single construct (Figure 2A), resulting in a dual plasmid system, allowing for the easy integration of other engineered translational elements if needed. We evaluated the incorporation efficiencies of the two new GCE systems (GCE v2.0 and GCE v2.5) and found that by adding a second copy of $tRNA^{CUA}$ (GCE v2.0), we achieved a five-fold improvement in the full length sfGFP compared to the original single tRNA system. Incorporating the engineered EF-Tu led to a modest further 1.5-fold improvement in sfGFP production (Figure 2B).

We tested the efficiency of GCE v2.0 by designing a sfGFP construct containing both amber and ochre nonsense codons (GFP-34TAG-150TAA) to direct the dual incorporation of

pAzF into a single protein. We observed reasonable suppression efficiency with GCE v2.0, highlighting the feasibility of the system for incorporating multiple ncAAs (Figure 2C).

SAGE enables high-throughput library-based GCE optimization directly in the host organism

Multi-component systems often require coordinated optimization of each component for optimal performance. While the LeuRS promoter facilitated robust performance, the absence of a clear RNA polymerase binding motif posed a challenge for engineering increased transcription. The synthetic *tac* promoter is broadly used in bacteria, provides strong expression, and is easily tunable due to its well characterized core promoter elements. Therefore, we evaluated the *tac* promoter[45] to replace the LeuRS promoter and support MjTyrRS expression for efficient ncAA incorporation into $sfGFP_{TAG150}$. Unexpectedly, sfGFP expression significantly decreased with the tac promoter compared to the endogenous LeuRS promoter (Figure 2E). This outcome aligns with observations by others that tuning the expression of GCE machinery that was originally developed for use in *E. coli* is crucial for robust GCE application in non-*E. coli* strains[40].

Rather than laboriously evaluating many promoter and ribosomal binding site variants individually to identify alternative promoters that enable improved performance, we leveraged the high transformation efficiency afforded by SAGE and the amenability of the sfGFP reporter assay to evaluate a large collection of *Mj*TyrRS expression variants in a pooled assay. We previously demonstrated the efficacy of SAGE for high-throughput sequencing-based methods to assess large promoter libraries in pooled assays. Adopting a similar approach, we aimed to optimize MjTyrRS by identifying regulatory elements that ensure sufficient MjTyrRS levels for robust ncAA incorporation without causing non-specific amino acid incorporation.

We constructed a pooled MjTyrRS expression library using a pool of 449 synthetic and natural promoter sequences. To achieve a diverse range of expression levels, we employed a cloning strategy to randomly incorporate one of 106 ribosomal binding site elements, designed by the RBS calculator to span approximately a 441-fold range of translational efficiency, downstream of the promoter sequences. Additionally, each regulatory sequence included the riboJ insulator sequence between the promoter and ribosomal binding site to stabilize gene expression. The resulting ~209,000 member MjTyrRS expression plasmid library was integrated into *Pseudomonas putida* using SAGE, resulting in a pooled collection of ~10,000,000 transformants strains, each containing a distinct promoter-RBS combination driving MjTyrRS expression, the reporter construct, and the dual $tRNA^{CUA}$ cassette from GCE 2.0 (Figure 2A).

Because the read-out for GCE efficiency is sfGFP, fluorescence activated cell sorting (FACS) can be performed on the strain library to identify efficient and orthogonal library members. This is done by first culturing the strain in the presence of the ncAA to select for efficient library members (positive sort) followed by culturing the positively sorted strain in the absence of ncAA (negative selection) to identify library members with high orthogonality (Figure 2D). For the initial positive selection, we cultivated the library in media containing pAzF and sorted the top 1.5% most fluorescent library members into a pooled library of strains. The pool of fluorescent cells was sub-cultured into fresh media lacking pAzF overnight. After the overnight cultivation, cells were sorted again via FACS. This time, members that exhibited no fluorescent signal above that of a *P. putida* strain lacking sfGFP were plate sorted individually into microtiter plates, cultivated overnight, sequenced and validated in GCE efficiency assays (Figure S2, Table S3).

The top performing strain displayed ncAA incorporation efficiency and orthogonality that was on par with GCE v2.5 (Figure 2E) despite lacking an engineered EF-Tu. Surprisingly, a

Lactobacillus_39770 promoter with relatively low transcriptional activity in other *Pseudomonas* sp. was identified in the top performing strain. Of note, this promoter was found to have between ~24 to 92-fold lower transcriptional activity than the *tac* promoter in our prior work, suggesting that poor performance with the *tac* promoter may be a consequence of excessive *Mj*TyrRS expression. The promoter was coupled with a ribosomal binding site element with a relatively high predicted RBS translation initiation rate of 67067.6, on par with the RBS from our tac system. Thus, this library selection method in one round of positive and negative sorting, produced a promoter/RBS pair with efficiency equivalent to the endogenous promoters, permitting the use of non-endogenous promoters to drive GCE technology.

SAGE facilitates the genetic code expansion of phylogenetically distant microbes

After successful implementation of GCE in *P. putida* KT2440, we evaluated the ability to easily transfer our optimized GCE systems into related Pseudomonas sp. (Figure 3A). These bacteria include the plant growth promoting rhizobacterium *P. fluorescens* strain SBW25[46] and two pseudomonads that were isolated from the endosphere of *Sorghum bicolor* under drought conditions[32, 47]. Each of the two, *P. frederiksbergensis* (TBS10)[32] and *P. facilor* (TBS28)[47], have been previously engineered to be compatible with SAGE via incorporation of a poly-attB landing site[32, 47].

We directly transferred the GCE v2.0 machinery developed in K2440 into the chromosomes of the three Pseudomonads and observed reasonable pAzF incorporation into sfGFP. This demonstrates that SAGE-based GCE systems can be shared across genetically similar bacteria (Figure 3D). Interestingly, even though the GCE efficiency was similar across the pseudomonads, the fluorescent output did vary across a ~2-fold range (Figure 3D). It remains to be seen whether these differences are a consequence of gene expression differences, or a consequence of another physiological trait such as ncAA transport.

A benefit of utilizing SAGE-based tools is the ability to easily transfer materials developed in SAGE-compatible hosts with phylogenetically distant SAGE-compatible bacteria. To demonstrate this benefit, we tested our the GCE 2.0 system in the actinomycete *Rhodococcus jostii* strain RHA1[48], a representative of a genus with diverse metabolic capabilities ranging from catabolism of cholesterol[49] and petroleum-derived hydrocarbon[50] to conversion of lignin-derived feedstocks into useful chemicals[51]. We evaluated GCE efficiency using the GCE v2.0 system to establish a baseline. GCE efficiency was not observed above background levels (Figure 3E), suggesting the machinery expression likely needed to be optimized.

To optimize expression, we identified the most abundant codon (Ala) in the RHA1 genome and utilized the endogenous aaRS and tRNA promoters associated with Ala to drive the GCE elements (Figure 3B). Considering the high GC content of Rhodococcus genomes and several strong codon biases, we also created a codon-optimized version of the protein elements to assess the impact of codon optimization on GCE efficiency. The RHA1-tailored system showed a dramatic improvement compared to GCE 2.0, with more subtle differences observed between codon-optimized and non-codon-optimized GCE-RHA1 systems (Figure 3B). However, the overall fluorescent output of the RHA1 system is comparable to GCE v1.0, suggesting potential for further improvement.

As mentioned above, the *p*CNF-RS used here is polyspecific, meaning it has the capacity to charge the $tRNA^{CUA}$ with several distinctive *para*-substituted phenylalanine analogs. However, each organism has its own distinct set of metabolite transporters, sensors, and other physiological

regulators that control expression of the proteins that enable ncAA uptake and it remains unclear how much of a role this plays in GCE efficiency with particular amino acids. To examine this, we utilized the permissivity of the pCNF-RS employed in our GCE system[34] to conduct a small ncAA screen, testing four additional *para*-substituted phenylalanine derivatives in both KT2440 and the environmental isolate TBS28. We compared their incorporation efficiencies to reported values in *E. coli*[34] (Figure 3F).

Overall, the relative incorporation efficiencies among the three organisms were similar, but with a few notable differences. Specifically, while both pseudomonads exhibited lower incorporation of 4-fluoro-L-phenylalanine relative to *E coli*, incorporation of this ncAA into sfGFP was almost non-existent in TBS28 (Figure 3F). These differences are unlikely to be due to the activity of the pCNF-RS, as the other ncAAs showed very similar efficiencies. It is more likely that differences in amino acid transport between the organisms are responsible. This underscores the importance of considering ncAA import mechanisms when integrating new bacterial strains.

Site specific incorporation of acetyl-L-lysine and other lysine analogs

We were encouraged by our initial success in the implementation and optimization of the *Mj*TyrRS-pCNF system and sought to broaden the existing lysine PTM interrogation toolkit in non-*E. coli* strains . As the *Mj*TyrRS system primarily incorporates aromatic ncAAs, we chose to onboard the pyrrolysyl-tRNA synthetase (PylRS) system. The pyrrolysyl-tRNA synthetase (PylRS)/$tRNA^{Pyl}$ pair, derived from *Methanosarcina* species, enables site-specific incorporation of lysine analogues due to the structural similarity between pyrrolysine—its natural substrate—and lysine[52]. Along with acetyl-L-lysine (AcK), a suite of ncAAs have been developed to interrogate lysine PTMs[35], and from these we chose to attempt to encode azido-lysine (AzK) and propargyloxycarbonyl-lysine (PlK)[35](Figure 4C). AcK incorporation enables direct interrogation of the influence of lysine acetylation on protein function both *in vivo* and *in vitro*[35]. Meanwhile AzK and PlK contain distinct bioorthogonal click chemistry handles[53] that can be used for various purposes – including probing protein interactions and fluorescent labeling. These lysine analogs have also been used to site specifically model ubiquitin[33].

We integrated the Pyl system in *P. putida* with two engineered pyrrolysine aminoacyl-tRNA synthetases (PylRS) by using the same genetic framework employed for GCE v2.0 (Figure 2A). The first, *Mb*PylRS(AF), contains active site mutations that permit the incorporation of bulky lysine analogues[54]. The second, chPylRS(IPYE), is an evolved synthetase known for its high efficiency in incorporating AcK in proteins in *E. coli*[55]. These aminoacyl-tRNA synthetases were paired with an evolved $tRNA^{Pyl}$, which has been shown to enhance AcK incorporation into proteins[31] (Figure 4A).

Incorporation of lysine analogues AzK and PlK with MbPylRS(AF) into sfGFP was successful with no additional alterations to the system. However, it was surprising to observe that, despite robust reported performance in *E. coli*, AcK incorporation efficiency was very low in *P. putida* (Figure 4B). We had previously observed that increasing *Mj*$tRNA^{Tyr}$ copy number enhanced pAzF incorporation efficiency and posited that $tRNA^{Pyl}$ copy number may also be limiting ncAA incorporation. To test this, we incorporated a second dual tRNA operon into the strain at a second *attB* site (GCE v3.0) and evaluated ncAA incorporation using both the *Mj*TyrRS-pCNF and chPylRS(IPYE).

Doubling the tRNA copy number improved ncAA with both systems, but to strikingly different extents. Given the already robust in incorporation of pAzF with the *Mj*TyrRS system, it

was unsurprising to see a substantial but relatively modest 2-fold increase in sfGFP production. However, incorporation of AcK by the chPylRS(IPYE) system was improved by 25-fold (Figure 4D), suggesting tRNA copy number was greatly limiting incorporation. This one improvement increased the efficiency of AcK incorporation to be on par with our best existing system and signifying that optimization of tRNA expression will be critical lever for optimization in each host.

Production of site-specially acetylated enolase in Pseudomonas putida with genetic code expansion.

While we were encouraged at the substantial improvement in GCE efficiency driven by additional copies of tRNA, we wanted to vet our system with an essential protein using biologically relevant potential acetylation sites. A previous proteomic analysis of acetylation of highly conserved lysines in central metabolic enzymes from diverse bacteria, including *Pseudomonas putida*[5], revealed that at least one critical conserved residue in the enolase enzyme can be acetylated *in vivo*. Enolase plays a crucial role in glycolysis and gluconeogenesis by catalyzing the reversible conversion of 2-phosphoglycerate to phosphoenolpyruvate, a key step in central carbon metabolism[5] and performs additional moonlighting functions that contribute to bacterial stress responses and pathogenicity[56]. As such, we selected the enolase enzyme as a model protein to test the efficiency of AcK incorporation at multiple highly conserved lysine residues.

The first conserved residue, K392 (Figure 4E) is involved in phosphoenolpyruvate catalysis and was observed to be acetylated in other bacteria in the tested conditions, but not in *Pseudomonas putida in the tested conditions*. On the other hand, another conserved residue at site K404 was found to be acetylated in the same test conditions. Site K392 is buried within the active site and, when acetylated, protrudes into the substrate[5] (Figure 4E). In contrast, site K404 is located more towards the periphery of the protein (Figure 4E).

P. putida encodes multiple lysine deacetylases, including those from the CobB and Metal-dependent lysine deacetylase families. Such deacetylases have a broad range of acetylated lysine substrates, but they are unable to deacetylate all acetylated lysine residues. We hypothesized that the lack of detectable acetylation at K392 may be due to efficient enzymatic deacetylation of one residue and not the other. By producing the acetylated protein *in vivo* in *Pseudomonas putida*, we could observe whether the modification is maintained at each residue over the course of a typical culturing experiment. If the acetylation remains stable, then that suggests the protein was simply not acetylated under the tested conditions.

For site-specific acetylated enolase production, we replaced the gene for $sfGFP_{TAG150}$ in GCE v3.0 with a series of enolase constructs ($Enolase_{WT}$, $Enolase_{TAG392}$ and $Enolase_{TAG404}$) in KT2440. Cultures for strains harboring each of these constructs were grown to stationary phase, at which point protein was extracted and affinity-purified to assess expression and acetylation of recombinant enolase. The three variants expressed successfully based on SDS-PAGE analysis (Figure 4F) and the intact molecular masses of all proteins were determined via mass spectrometric analysis. This analysis revealed masses corresponding to acetyl lysine incorporation for $Enolase_{TAG392}$ and $Enolase_{TAG404}$ (Figure 4G). While the molecular weights for other contaminating proteins were detected, the mass associated with $Enolase_{WT}$, was not observed in the acetylated enolase samples (Figure S4). While not exhaustive, this data refutes the hypothesis that intrinsic lysine deacetylase activity during the cultivation was responsible for the lack of acetylation at K392. In summary, we have successfully pioneered acetyl-lysine incorporation in a non-*E. coli*

strain and developed a broadly applicable approach to establish genetic code expansion in non-model organisms.

DISCUSSION

Genetic code expansion has revolutionized the analysis of the bacterial acetylome by enabling the precise incorporation of PTMs along with a suite of PTM enrichment and visualization tools, enabling real-time monitoring of acetylation dynamics under physiological conditions. However, inconsistent genetic tractability and unpredictable translational regulatory elements across microbes have hindered the implementation and optimization of this technology in diverse bacteria, particularly those of interest for human health and bioremediation. This is most evident with respect to the ncAA acetyl lysine itself, as the subtlety of the modification makes it a more challenging incorporation target.

We address this challenge by integrating GCE with serine recombinase-assisted genome engineering (SAGE), a method renowned for its high efficiency across a wide range of bacterial strains. With GCE-SAGE, each GCE component is site-specifically integrated into the bacterial genome at a high enough efficiency for library optimization and with enough landing pads (attB sites) to integrate up to ten constructs genetically. This strategy allowed for the stable integration of GCE components into the genome of Pseudomonas putida KT2440 and improved efficiency by easily allowing for increased $tRNA^{CUA}$ copy number. SAGE also enabled development of a high-throughput promoter and ribosome binding site (RBS) library selection method using fluorescence-activated cell sorting (FACS). This approach identified highly efficient promoter/RBS pairs, facilitating the fine-tuning of gene expression in non-model organisms. This technique is crucial for matching GCE output to endogenous production levels, especially when only synthetic promoters or unknown promoter strengths are available.

GCE-SAGE was then successfully transferred to multiple Proteobacteria (*Pseudomonas fluorescens* SBW25, *Pseudomonas frederiksbergensis* TBS10, and *Pseudomonas facilor* TBS28) and the Actinobacterium Rhodococcus jostii RHA1. Screening four para-substituted phenylalanine derivatives revealed organism-specific differences in incorporation efficiency, likely due to variations in amino acid transport rather than pCNF-RS activity. Studying and expressing amino acid transporters will be a critical component to enhance ncAA uptake as SAGE- enables application of in GCE in new model systems.

We successfully incorporated lysine analogs (AzK, PrK, and AcK) using evolved pyrrolysyl-tRNA synthetases (PylRS). The variable efficiency of incorporation, particularly for AcK, highlighted the need for additional tRNA copies to achieve biologically relevant levels, confirming the critical role of tRNA abundance in GCE performance. It was encouraging that the efficiency of the system could be enhanced from near zero levels by simply adding additional copies of tRNA. As this has been observed in mammalian systems as well, it is likely that this optimization approach is near universal, providing a simple path towards GCE optimization.

The stable incorporation of acetyl-lysine at two distinct sites (K392 and K404) in the essential glycolytic enzyme enolase in Pseudomonas putida showcased the practical utility of our optimized GCE platform. In conclusion, we have successfully pioneered the establishment of acetylation in diverse bacterial strains, developed a host-agnostic GCE platform and identified strategies to optimize GCE efficiency in the hosting organism. These advancements herald new

opportunities for studying PTMs in bacteria, unlocking numerous possibilities for both fundamental research and industrial biotechnology applications

ACKNOWLEDGEMENTS

The research described in this paper is a part the Predictive Phenomics Initiative at Pacific Northwest National Laboratory and conducted under the Laboratory Directed Research and Development Program. Additional support was provided by the U.S. Department of Energy (DOE), Office of Biological and Environmental Research (BER), as part of BER's Genomic Science Program (GSP), and is a contribution of the Pacific Northwest National Laboratory (PNNL) Secure Biosystems Design Science Focus Area "Persistence Control of Engineered Functions in Complex Soil Microbiomes". Pacific Northwest National Laboratory is a multiprogram national laboratory operated by Battelle for the U.S. Department of Energy under Contract No. DE-AC05-76RL01830. We also thank Adam Guss for the sharing the SAGE-compatible *Pseudomonas putida* strain AG5577 and Alan Wolfe for insightful conversations regarding lysine acetylation in bacterial proteins.

MATERIALS AND METHODS

Reagents

All commercial chemicals are of reagent grade or higher. All solutions were prepared in deionized water that was further treated by Barnstead Nanopure® ultrapure water purification system (Thermo Fisher Scientific). *Pseudomonas putida* AG5577, a derivative of KT2440 with multiple *attB* sites for compatibility with SAGE, was provided by the Adam Guss. The strain was routinely cultured at 30 °C on LB agar plates or in LB liquid medium. Antibiotics were added where appropriate to following final concentrations: kanamycin sulfate (50 µg/ml), apramycin sulfate (50 µg/ml), carbenicillin (50 µg/ml), gentamicin sulfate (15 µg/ml), neomycin sulfate (10 µg/ml), or spectinomycin/streptomycin (200/300 mg/L, respectively)] Non-canonical amino acids 4-azido-L-phenylalanine (AzF), Acetyl-L-lysine (AcK) and N6-((Prop-2-yn-1-yloxy)carbonyl)-L-lysine hydrochloride (PlK) were purchased from Chem Impex, 4-Fluoro-L-phenylalanine (4FF), *p*-chlorophenylalanine (4ClF), 4-benzoyl-L-phenylalanine (BzF), *p*-Acetylphenylalanine and 4-Propargyloxy-L-phenylalanine were purchased from Cayman Chemicals and N6-((2-Azidoethoxy)carbonyl-L-lysine was purchased from Sigma Aldrich. Aromatic ncAAs were dissolved in equimolar NaOH to make 100 mM stock solutions. Lysine derivative ncAAs were dissolved in ddH2O to make 200 mM stock solutions. Solutions of antibiotics and unAAs were filtered through 0.22 µm sterile membrane filters.

General culturing conditions and media

The strains and plasmids used in this study are listed in table S1. Routine cultivation of *E. coli* for plasmid construction and maintenance was performed at 37°C using LB (Lennox) medium supplemented with antibiotics kanamycin sulfate (50 µg/ml), apramycin sulfate (50 µg/ml), carbenicillin (50 µg/ml), gentamicin sulfate (15 µg/ml), neomycin sulfate or spectinomycin/streptomycin (200/300 mg/L, respectively) and agar (15 g/liter; for solid medium). All pseudomonad and *R. jostii* cultures were incubated at 30°C unless otherwise indicated. Cultures were incubated in 24-well deep well plates with shaking at 700 rpm in an heated plate shaker (Southwest Science).

LB (Lennox) was used for routine pseudomonad strain maintenance and competent cell preparations. Kanamycin sulfate (50 µg/ml), apramycin sulfate (50 µg/ml), carbenicillin (50 µg/ml), gentamicin sulfate (15 µg/ml), or spectinomycin/streptomycin (200/300 mg/L, respectively) were used for antibiotic selection. LB (Lennox) or R2A medium was used for routine *R. jostii* strain maintenance and competent cell preparations. Apramycin sulfate (30 µg/ml) or neomycin sulfate (10 µg/ml) were used for antibiotic selection. All solid medium was prepared by addition of agar (15 g/liter).

MOPS (3-(N-morpholino)propanesulfonic acid))-based mineral medium (MME) supplemented with 10 mM NH4Cl and with 10 mM glucose were used for pseudomonad GCE experiments. MME contains 9.1 mM K_2HPO_4, 20 mM Mops, 4.3 mM NaCl, 20 mM NH_4Cl, 0.41 mM MgSO4, 68 µM $CaCl_2$, and 1× MME trace minerals (pH adjusted to 7.0 with KOH). MME trace mineral stock solution (1000×) contains per liter 1 ml of concentrated HCl, 0.5 g of Na_4EDTA, 2 g of $FeCl_3$, and 0.05 g each of H_3BO_3, $ZnCl_2$, $CuCl_2{\cdot}2H_2O$, $MnCl_2{\cdot}4H_2O$, $(NH_4)_2MoO_4$, $CoCl_2{\cdot}6H_2O$, and $NiCl_2{\cdot}6H_2O$. An MME variant (MMV) additionally containing 10 mg each of niacin, pantothenate, lipoic acid, p-aminobenzoic acid, thiamine (B1), riboflavin (B2), pyridoxine (B6), and cobalamin (B12) and 4 mg each of biotin and folic acid per liter was used for *R. jostii* assays.

Plasmid construction

Q5 High-Fidelity DNA Polymerase [New England Biolabs (NEB)] and primers synthesized by Eurofins Genomics were used in all PCR amplifications for plasmid construction. OneTaq DNA polymerase (NEB) was used for colony PCR. EvaGreen dye (Biotium) was supplemented at 1× final concentration in PCRs for quantitative PCR (qPCR) applications. Plasmids constructed by Gibson Assembly using the NEBuilder HiFi DNA Assembly Master Mix (NEB) or ligation using T4 DNA ligase (NEB). Plasmids were transformed into competent NEB 5-alpha F'I^q (NEB). Standard chemically competent E. coli transformation protocols were used to construct plasmid host strains. Transformants were selected on LB (Lennox) agar plates containing antibiotics [kanamycin sulfate (50 µg/ml), apramycin sulfate (50 µg/ml), carbenicillin (50 µg/ml), gentamicin sulfate (15 µg/ml), neomycin sulfate or spectinomycin/streptomycin (XX mg/L)] for selection and incubated at 37°C. Template DNA for PCRs synthesized by Twist Biosciences. The Zymoclean Gel DNA recovery kit (Zymo Research) was used for all DNA gel purifications. Plasmid DNA was purified from E. coli using the GeneJet plasmid miniprep kit (Thermo Fisher Scientific) or the ZymoPURE II plasmid midiprep kit (Zymo Research). Sequences of plasmids were confirmed using Sanger sequencing performed by Eurofins Genomics or nanopore sequencing by Plasmidsaurus. Plasmids used in this work are listed in table S1, and maps of plasmids constructed in this study can be found in Supplemental File P1.

Strain construction

All genome modifications were performed by integration of non-replicating plasmids into the chromosome with serine recombinases via SAGE, where Bxb1, R4, or Tg1 integrases unidirectionally recombine DNA between cognate attB and attP sequences. Plasmids containing GCE machinery harbor either a Bxb1, R4 or Tg1 attP sequence, and variants of *Pseudomonas putida* KT2440 (AG5577), *Pseudomonas fluorescens* SBW25 (JE4621), *Pseudomonas fredericksbergensis* TBS10 (JE5041), *Pseudomonas facilor* TBS28 (RS175) and *Rhodococcus jostii* RHA1 have each been engineered to harbor the cognate Bxb1, R4 or Tg1 attB sequence.

Mutant strains and the plasmids used for each gene deletion or gene insertion are listed in Table S1 and S2, respectively.

Plasmid transformations were performed using electroporation with electrocompetent cells. Electrocompetent cells were prepared by growing cultures as previously described[32]. in LB or R2A broth (for pseudomonads or RHA1 respectively) to until cultures reached stationary phase. Fresh medium was inoculated with the preculture to an OD_{600} of 0.01 and incubated aerobically until the cells reached a mid-log phase (~OD_{600} = 0.4 to 0.6). Once the desired culture density was reached, the cells were centrifuged at 5000*g* for 20 min at 4°C and washed at one-half culture volume of ice-cold 10% glycerol. Centrifugation and washing were repeated two additional times, and then cells were resuspended in 1/50th culture volume of ice-cold 10% glycerol. Competent cells were either used immediately or stored at −80°C.

Electroporation was performed as follows. GCE machinery and SAGE integrase plasmids (200 ng each) were added to 70 µL of ice-cold electrocompetent cells with the total volume of DNA not exceeding 5 uL. Competent cells were transferred into an ice-cold 0.1-cm-gap electroporation cuvette and electroporated at 1.6 kV, 25 µF, and 200 ohm. Following electroporation, 950 µL of SOC or R2A were added to the competent cells, and the resulting mixture was incubated aerobically, at 30°C with shaking for 3 hours. Following this recovery step, various dilutions of recovery cultures were plated on selective LB or R2A solid medium and incubated aerobically at 30°C. Primers used to screen for integration of the poly-*attP* cassette insertions in pseudomonads and *R. jostii* can be found in Table S6. Verified strains were stored at -80 C with 20% glycerol.

GCE incorporation efficiency assays

Starter cultures for pseudomonads and RHA1 were prepared by inoculating 6 mL of LB or R2A media lacking antibiotic with appropriate strains from glycerol stocks. These strains were cultivated to stationary phase at 30°C with shaking until the cultures reached saturation (20 hours for P. fluorescens and ~XX hours for R. jostii). After stationary phase was reached, cultures were diluted 100-fold into 6 mL of MME with 10 mM NH4Cl and with 10 mM glucose lacking antibiotic and incubated again at 30°C with shaking until the cultures reached saturation. The saturated cultures were used in GCE efficiency assays. All GCE assays were performed in 24-well deep well plates with shaking at 30C (800 rpm, 1-mm orbital). The media used in assays was composed of MME with 10 mM NH4Cl, 10 mM glucose, and a 1× 18-amino acid solution. Each strain was tested in quadruplicate under two conditions: with and without ncAA supplementation (+/− ncAA). For -ncAA cultures, no additional ncAA was added. For +ncAA cultures, either 1 mM ncAA for Mj system ncAAs or 10 mM ncAA for Pyl system ncAAs was also added to the media. Saturated cultures prepared as described above were used to inoculate 2mL of the assay media for a 100-fold dilution. Cultures incubated for 24 hours, after which cultures were diluted 100-fold in 1× PBS, and fluorescence was measured using a NovoCyte flow cytometer (Acea Biosciences). Green fluorescence (mNeonGreen) was measured using a 488-nm laser with a 530/30-nm filtered detector. A preliminary gating of 2500 and 10 were used for forward scatter (FSC) and side scatter (SSC), respectively, and a total of 25,000 events were measured for each sample.

Creation of Promoter-RBS library

A combination of 449 synthetic and natural promoter sequences (Table S4 - promoters) were synthesized with the following parameters and coupled with 1 of 106 synthetic ribosomal

binding sites designed by the RBS calculator (Table S5 – RBSs). Synthetic promoters were derived from commonly used promoters in the field of synthetic biology, as well as custom promoters generated for this study. Each promoter was coupled with a downstream synthetic RBS, designed by the RBS calculator to span a 441-fold range of translation initiation rates, during the cloning process. Promoter sequence DNA, as well as flanking sequences used for cloning, were synthesized as a pool of oligos by Twist Biosciences. To generate a *Mj*TyrRS expression variant plasmid library primers oPNL2125 / oPNL2126 were used to amplify the backbone of pJE2027, excising the existing tac promoter and RBS. The promoter library was amplified using forward primer oPNL2127 and an equimolar amount of six reverse primers that each contain a priming sequence that binds to the oligo pool, one of six sets of degenerate RBS sequences, and a region of homology with the plasmid backbone. The plasmid backbone and promoter/RBS pool were amplified using Q5 hot start high-fidelity 2x master mix (New England Biolabs). PCR products were assembled using NEB HiFi DNA assembly master mix (New England Biolabs) and transformed into chemically competent NEB 5-alpha F'IQ competent cells and recovered in 1 ml of SOC at 37 °C for 1 hour. A 10-µl aliquot of the recovery mixture was diluted and plated on LB + kanamycin sulfate (50 µg/ml) to determine the cloning efficiency and library coverage, and the remaining 990 µL was propagated through overnight liquid selections using 50 ml LB + kanamycin sulfate (50 µg/ml) grown at 37 °C, 200 rpm. The resulting plasmid library contained ~209,000 transformants. Plasmid DNA was then extracted from library cultures with a ZymoPURE II Midiprep kit (Zymo Research) for subsequent transformation into final the host strains. Oligo sequences are found in Table S6.

The plasmid pool was integrated into the R4 *attB* site in the chromosome of *P. putida* GCE1 (AG5577-derivative containing pEVF108 at the Bxb1 *attB* site) by co-electroporation of 500 ng of the plasmid pool with 3 ug of pGW38 (R4 integrase expression plasmid) into 50 µL of electrocompetent cells. The electroporated cells were resuspended in 950 µL of SOC, incubated at 30°C for 1 hour with shaking. As above, dilutions generated from 10 µL of the recovery culture were plated onto LB supplemented with kanamycin sulfate (50 µg/ml), and resulting colonies were quantified to identify the size of the library. The remaining 990 µL was propagated through overnight liquid selections using 50 ml LB + kanamycin sulfate (50 µg/ml) grown at 30 °C, 200 rpm. Library cultures were diluted to OD_{600} = 1 with glycerol to a final concentration of 12.5% glycerol and stocked as 1-ml aliquots for use in subsequent experiments.

Identification of active GCE-SAGE system with FACS-based selection

A fluorescence-activated cell sorting (FACS)-based strategy was used to enrich and refine a *Pseudomonas putida* KT2440 promoter library based on green fluorescent protein (GFP) expression. The promoter library was introduced into *P. putida* KT2440 via electroporation as described above and glycerol stocks of the library were revived for selections. This was done by inoculating 50 mL of LB media with one 1mL aliquot of the prepared glycerol stocks and incubating at 30C for at least 6 hours. After, the culture was washed in MME (1X, 4 min at 5000 rcf) and resuspended in 50 mL MME with 10 mM glucose and incubated overnight at 30C overnight.

This overnight culture was used to inoculate a 24-well deep well plate containing 2mL MME with 10 mM NH4Cl, 10 mM glucose, and a 1× 18-amino acid solution as described above. This block contained wells with and without 1 mM pAzF for negative and positive selections of the library. The plate was also inoculated with robust system GCE v2 in the presence and absence of ncAA to provide fluorescent benchmarks for gating negative and positive events. Lastly the

plate contained the parent strain AG5577 to establish background fluorescence. The plate was incubated overnight with shaking at 30C (800 rpm, 1-mm orbital).

Positive selection

The Sony SH800 cell sorter was used for all sorting experiments with a four-laser set up (405, 488, 561, and 638 nm) and a 100-um sorting chip. The samples were sorted using the "Normal" sort mode into two-way 1.5 mL tubes using a forward scatter (FSC) threshold value of 0.05%. Initial gates were established on forward scatter—area by back scatter—area (FSC-A x BSC-A) and then forward scatter—height by forward scatter—width (FSC-H and FSC-W) to select for cells of expected size. The third gate was established with both the parent strains and the -ncAA condition for GCE v2 as a no-fluorescence control. Lastly, a fourth gate was drawn using the +ncAA condition to map out the range of GCE-produced fluorescence.

With these gates, the library incubated in the presence and absence of ncAA was analyzed. A ncAA-insensitive high fluorescence peak was observed in both populations, indicative of library members that may dysregulate GCE systems and charge native amino acids. A gate capturing the top 1% of events for the +ncAA library but avoiding the ncAA-insensitive events was drawn, and 1,000 of those events were bulk-sorted into a 1.5 mL Eppendorf tube for a positive selection. 1 mL of LB media was added to the tube and the positive library was incubated at 30C to recover for two hours. After, 50 mL of MME with 10 mM glucose was inoculated with the recovered library and cultured for 48 hours at 30C.

Negative selection

After incubation, the positive library was sub-cultured into fresh MME with 10 mM glucose at a 50-fold dilution and incubated overnight with shaking at 30C. This culture was analyzed by the Sony SH800 cell sorter and low background events as determined by gating from the parent strain and GCE v2.0 in the -ncAA condition. Low background events were single-cell sorted with high purity into a 96 well plate containing 150 uL of LB media. Controls, including the parent strain, and GCE v2.0 were also added to the plate to provide direct comparisons during validation. The plate was incubated with shaking at 30 C overnight, then used to inoculate a 96-deep well plate for glycerol stocks as well as a 96 well plate containing 150 uL of MME with 10 mM glucose for validations assays.

Validation experiments

After incubation overnight at 30C with shaking, the above plate was used to inoculate two additional black-walled, clear-bottom 96-well microplates, one containing 150 uL of MME-GCE without ncAA to determine background incorporation of the potential hits and one with MME-GCE containing 1 mM pAzF to determine GCE efficiency. These plates were incubated for 24 hours using the "fast shaking" 1 mM double orbital setting on a Neo2SM plate reader (BioTek). Fluorescence ($F_{501,520}$ for sfGFP) was then measured for both plates. Background fluorescence readings from wells containing the non-fluorescent parent strain were averaged and subtracted from sample readings before analysis. A subset of potential hits from the initial block were then screened in a typical GCE experiment using 2 mL of culture (see methods above) and promising clones were sequenced.

Expression and purification of ncAA-protein for mass spectrometry analysis

Cell pellets were resuspended in a lysis/wash buffer [50 mM tris, 500 mM NaCl, and 5 mM imidazole (pH 7.5)] and lysed via sonication. Cell debris was pelleted at 15,000 rcf for 25 min at

4°C and clarified cell lysate was recovered. To bind His_6-tagged protein, clarified cell lysate was incubated with 200 µL of Ni-NTA resin (HisPur™ Ni-NTA Resin, Thermo Scientific) at 4°C for 1 hour with rocking. Resin was collected and extensively washed with 50 resin bed volumes (bv) of lysis buffer. Bound protein was eluted from the resin by incubation with 5 bv of elution buffer (lysis buffer with 200 mM imidazole) concentrated and exchanged into storage buffer (50 mM phosphate, 150 mM NaCl) with a 3-kDa MWCO Vivaspin spin-concentration filter (GE Health Sciences). Protein concentration was determined by absorbance at 280 nm, flash-frozen with liquid nitrogen and stored at −80°C until needed. For purification of $sfGFP_{2XpAzF}$ an additional size exclusion chromatography step was added. However, during analysis, $sfGFP_{2XpAzF}$ experienced some proteolytic degradation, though maintained its fluorescent signature (Figure S4). $sfGFP_{2XpAzF}$ was purified and submitted for MS analysis.

For mass analysis of protein, the purified proteins were then analyzed by Creative Proteomics facility on a Synapt G2-Si mass spectrometer by the following method. The protein of interest was isolated using chromatographic techniques (C4 on the H-Class UPLC) and introduced to the Synapt G2-Si using a dual orthogonal API source (Lock- Spray ESI/APCI) and subjected to CID fragmentation. The mass spectrometer was operated in ESI positive resolution mode in the range 300-5000 Da. The capillary voltage was set to 3.0 kV with a sampling cone voltage of 78 V, a source temperature of 150°C and a desolvation temperature of 550°C. The cone gas was to set to 0 L/h with desolvation gas at 300 L/h and the nebulizer set to 6.0 bar. The protein's molecular weight can then be determined by deconvoluting the fragment masses using Waters MaxEnt software.

REFERENCES

1. Cain JA, Solis N, Cordwell SJ. Beyond gene expression: the impact of protein post-translational modifications in bacteria. J Proteomics. 2014;97:265-86. Epub 20130828. doi: 10.1016/j.jprot.2013.08.012. PubMed PMID: 23994099.

2. Macek B, Forchhammer K, Hardouin J, Weber-Ban E, Grangeasse C, Mijakovic I. Protein post-translational modifications in bacteria. Nat Rev Microbiol. 2019;17(11):651-64. Epub 20190904. doi: 10.1038/s41579-019-0243-0. PubMed PMID: 31485032.

3. Christensen DG, Xie X, Basisty N, Byrnes J, McSweeney S, Schilling B, Wolfe AJ. Post-translational Protein Acetylation: An Elegant Mechanism for Bacteria to Dynamically Regulate Metabolic Functions. Front Microbiol. 2019;10:1604. Epub 20190712. doi: 10.3389/fmicb.2019.01604. PubMed PMID: 31354686; PMCID: PMC6640162.

4. Li Z, Wang Y, Yao Q, Justice NB, Ahn TH, Xu D, Hettich RL, Banfield JF, Pan C. Diverse and divergent protein post-translational modifications in two growth stages of a natural microbial community. Nat Commun. 2014;5:4405. Epub 20140725. doi: 10.1038/ncomms5405. PubMed PMID: 25059763; PMCID: PMC4279252.

5. Nakayasu ES, Burnet MC, Walukiewicz HE, Wilkins CS, Shukla AK, Brooks S, Plutz MJ, Lee BD, Schilling B, Wolfe AJ, Muller S, Kirby JR, Rao CV, Cort JR, Payne SH. Ancient Regulatory Role of Lysine Acetylation in Central Metabolism. mBio. 2017;8(6). Epub 20171128. doi: 10.1128/mBio.01894-17. PubMed PMID: 29184018; PMCID: PMC5705920.

6. Liu M, Guo L, Fu Y, Huo M, Qi Q, Zhao G. Bacterial protein acetylation and its role in cellular physiology and metabolic regulation. Biotechnol Adv. 2021;53:107842. Epub 20211006. doi: 10.1016/j.biotechadv.2021.107842. PubMed PMID: 34624455.

7. Rizo J, Encarnación-Guevara S. Bacterial protein acetylation: mechanisms, functions, and methods for study. Front Cell Infect Microbiol. 2024;14:1408947. Epub 20240704. doi: 10.3389/fcimb.2024.1408947. PubMed PMID: 39027134; PMCID: PMC11254643.

8. Lammers M. Post-translational Lysine Ac(et)ylation in Bacteria: A Biochemical, Structural, and Synthetic Biological Perspective. Front Microbiol. 2021;12:757179. Epub 20211011. doi: 10.3389/fmicb.2021.757179. PubMed PMID: 34721364; PMCID: PMC8556138.

9. Liu X, Yang M, Ge F, Zhao J. Lysine acetylation in cyanobacteria: emerging mechanisms and functions. Biochem Soc Trans. 2025;53(1). Epub 20250212. doi: 10.1042/bst20241037. PubMed PMID: 39936403.

10. Zhang J, Sprung R, Pei J, Tan X, Kim S, Zhu H, Liu CF, Grishin NV, Zhao Y. Lysine acetylation is a highly abundant and evolutionarily conserved modification in Escherichia coli. Mol Cell Proteomics. 2009;8(2):215-25. Epub 20080823. doi: 10.1074/mcp.M800187-MCP200. PubMed PMID: 18723842; PMCID: PMC2634580.

11. Popova L, Carr RA, Carabetta VJ. Recent Contributions of Proteomics to Our Understanding of Reversible N(ε)-Lysine Acylation in Bacteria. J Proteome Res. 2024;23(8):2733-49. Epub 20240305. doi: 10.1021/acs.jproteome.3c00912. PubMed PMID: 38442041; PMCID: PMC11296938.

12. Weinert BT, Iesmantavicius V, Wagner SA, Scholz C, Gummesson B, Beli P, Nystrom T, Choudhary C. Acetyl-phosphate is a critical determinant of lysine acetylation in E. coli. Mol Cell. 2013;51(2):265-72. Epub 20130703. doi: 10.1016/j.molcel.2013.06.003. PubMed PMID: 23830618.

13. Schilling B, Christensen D, Davis R, Sahu AK, Hu LI, Walker-Peddakotla A, Sorensen DJ, Zemaitaitis B, Gibson BW, Wolfe AJ. Protein acetylation dynamics in response to carbon overflow in Escherichia coli. Mol Microbiol. 2015;98(5):847-63. Epub 20150910. doi: 10.1111/mmi.13161. PubMed PMID: 26264774; PMCID: PMC4715485.

14. Kuhn ML, Zemaitaitis B, Hu LI, Sahu A, Sorensen D, Minasov G, Lima BP, Scholle M, Mrksich M, Anderson WF, Gibson BW, Schilling B, Wolfe AJ. Structural, kinetic and proteomic characterization of acetyl phosphate-dependent bacterial protein acetylation. PLoS One. 2014;9(4):e94816. Epub 20140422. doi: 10.1371/journal.pone.0094816. PubMed PMID: 24756028; PMCID: PMC3995681.

15. Ren J, Sang Y, Lu J, Yao YF. Protein Acetylation and Its Role in Bacterial Virulence. Trends Microbiol. 2017;25(9):768-79. Epub 20170424. doi: 10.1016/j.tim.2017.04.001. PubMed PMID: 28462789.

16. Venkat S, Chen H, Stahman A, Hudson D, McGuire P, Gan Q, Fan C. Characterizing Lysine Acetylation of Isocitrate Dehydrogenase in Escherichia coli. J Mol Biol. 2018;430(13):1901-11. Epub 20180504. doi: 10.1016/j.jmb.2018.04.031. PubMed PMID: 29733852; PMCID: PMC5988991.

17. Venkat S, Gregory C, Meng K, Gan Q, Fan C. A Facile Protocol to Generate Site-Specifically Acetylated Proteins in Escherichia Coli. J Vis Exp. 2017(130). Epub 20171209. doi: 10.3791/57061. PubMed PMID: 29286490; PMCID: PMC5755542.

18. Venkat S, Nannapaneni DT, Gregory C, Gan Q, McIntosh M, Fan C. Genetically encoding thioacetyl-lysine as a non-deacetylatable analog of lysine acetylation in Escherichia coli. FEBS Open Bio. 2017;7(11):1805-14. Epub 20171016. doi: 10.1002/2211-5463.12320. PubMed PMID: 29123988; PMCID: PMC5666399.

19. Chen H, Venkat S, Hudson D, Wang T, Gan Q, Fan C. Site-Specifically Studying Lysine Acetylation of Aminoacyl-tRNA Synthetases. ACS Chem Biol. 2019;14(2):288-95. Epub 20190129. doi: 10.1021/acschembio.8b01013. PubMed PMID: 30642164.

20. Araujo J, Ottinger S, Venkat S, Gan Q, Fan C. Studying Acetylation of Aconitase Isozymes by Genetic Code Expansion. Front Chem. 2022;10:862483. Epub 20220324. doi: 10.3389/fchem.2022.862483. PubMed PMID: 35402385; PMCID: PMC8987015.

21. Venkat S, Gregory C, Sturges J, Gan Q, Fan C. Studying the Lysine Acetylation of Malate Dehydrogenase. J Mol Biol. 2017;429(9):1396-405. Epub 20170331. doi: 10.1016/j.jmb.2017.03.027. PubMed PMID: 28366830; PMCID: PMC5479488.

22. Wang Q, Zhang Y, Yang C, Xiong H, Lin Y, Yao J, Li H, Xie L, Zhao W, Yao Y, Ning ZB, Zeng R, Xiong Y, Guan KL, Zhao S, Zhao GP. Acetylation of metabolic enzymes coordinates carbon source utilization and metabolic flux. Science. 2010;327(5968):1004-7. doi: 10.1126/science.1179687. PubMed PMID: 20167787; PMCID: PMC4183141.

23. Kremer M, Schulze S, Eisenbruch N, Nagel F, Vogt R, Berndt L, Dorre B, Palm GJ, Hoppen J, Girbardt B, Albrecht D, Sievers S, Delcea M, Baumann U, Schnetz K, Lammers M. Bacteria employ lysine acetylation of transcriptional regulators to adapt gene expression to cellular metabolism. Nat Commun. 2024;15(1):1674. Epub 20240223. doi: 10.1038/s41467-024-46039-8. PubMed PMID: 38395951; PMCID: PMC10891134.

24. Feid SC, Walukiewicz HE, Wang X, Nakayasu ES, Rao CV, Wolfe AJ. Regulation of Translation by Lysine Acetylation in Escherichia coli. mBio. 2022;13(3):e0122422. Epub 20220523. doi: 10.1128/mbio.01224-22. PubMed PMID: 35604121; PMCID: PMC9239087.

25. Luu J, Carabetta VJ. Contribution of N(epsilon)-lysine Acetylation towards Regulation of Bacterial Pathogenesis. mSystems. 2021;6(4):e0042221. Epub 20210824. doi: 10.1128/mSystems.00422-21. PubMed PMID: 34427523; PMCID: PMC8407419.

26. Fang Z, Lai F, Cao K, Zhang Z, Cao L, Liu S, Duan Y, Yin X, Ge R, He QY, Sun X. Potential Role of Lysine Acetylation in Antibiotic Resistance of Escherichia coli. mSystems. 2022;7(6):e0064922. Epub 20221026. doi: 10.1128/msystems.00649-22. PubMed PMID: 36286553; PMCID: PMC9765299.

27. Wang S, Osgood AO, Chatterjee A. Uncovering post-translational modification-associated protein-protein interactions. Curr Opin Struct Biol. 2022;74:102352. Epub 20220322. doi: 10.1016/j.sbi.2022.102352. PubMed PMID: 35334254; PMCID: PMC9464464.

28. Knyphausen P, Lang F, Baldus L, Extra A, Lammers M. Insights into K-Ras 4B regulation by post-translational lysine acetylation. Biol Chem. 2016;397(10):1071-85. doi: 10.1515/hsz-2016-0118. PubMed PMID: 27176741.

29. Kirchgassner S, Braun MB, Bartlick N, Koc C, Reinkemeier CD, Lemke EA, Stehle T, Schwarzer D. Synthesis, Biochemical Characterization, and Genetic Encoding of a 1,2,4-Triazole Amino Acid as an Acetyllysine Mimic for Bromodomains of the BET Family. Angew Chem Int Ed Engl. 2023;62(12):e202215460. Epub 20230209. doi: 10.1002/anie.202215460. PubMed PMID: 36585954.

30. Zhang ZJ, Pedicord VA, Peng T, Hang HC. Site-specific acylation of a bacterial virulence regulator attenuates infection. Nat Chem Biol. 2020;16(1):95-103. Epub 20191118. doi: 10.1038/s41589-019-0392-5. PubMed PMID: 31740807; PMCID: PMC8439376.

31. Fan C, Xiong H, Reynolds NM, Soll D. Rationally evolving tRNAPyl for efficient incorporation of noncanonical amino acids. Nucleic Acids Res. 2015;43(22):e156. Epub 20150806. doi: 10.1093/nar/gkv800. PubMed PMID: 26250114; PMCID: PMC4678846.

32. Elmore JR, Dexter GN, Baldino H, Huenemann JD, Francis R, Peabody GLt, Martinez-Baird J, Riley LA, Simmons T, Coleman-Derr D, Guss AM, Egbert RG. High-throughput genetic engineering of nonmodel and undomesticated bacteria via iterative site-specific genome integration. Sci Adv. 2023;9(10):eade1285. Epub 20230310. doi: 10.1126/sciadv.ade1285. PubMed PMID: 36897939; PMCID: PMC10005180.

33. Shandell MA, Tan Z, Cornish VW. Genetic Code Expansion: A Brief History and Perspective. Biochemistry. 2021;60(46):3455-69. Epub 20210701. doi: 10.1021/acs.biochem.1c00286. PubMed PMID: 34196546; PMCID: PMC8613843.

34. Young DD, Young TS, Jahnz M, Ahmad I, Spraggon G, Schultz PG. An evolved aminoacyl-tRNA synthetase with atypical polysubstrate specificity. Biochemistry. 2011;50(11):1894-900. Epub 20110201. doi: 10.1021/bi101929e. PubMed PMID: 21280675; PMCID: PMC3694404.

35. Neumann-Staubitz P, Lammers M, Neumann H. Genetic Code Expansion Tools to Study Lysine Acylation. Adv Biol (Weinh). 2021;5(12):e2100926. Epub 20211028. doi: 10.1002/adbi.202100926. PubMed PMID: 34713630.

36. de Lorenzo V, Perez-Pantoja D, Nikel PI. Pseudomonas putida KT2440: the long journey of a soil-dweller to become a synthetic biology chassis. J Bacteriol. 2024;206(7):e0013624. Epub 20240708. doi: 10.1128/jb.00136-24. PubMed PMID: 38975763; PMCID: PMC11270871.

37. Bagdasarian M, Lurz R, Ruckert B, Franklin FC, Bagdasarian MM, Frey J, Timmis KN. Specific-purpose plasmid cloning vectors. II. Broad host range, high copy number, RSF1010-derived vectors, and a host-vector system for gene cloning in Pseudomonas. Gene. 1981;16(1-3):237-47. doi: 10.1016/0378-1119(81)90080-9. PubMed PMID: 6282695.

38. Martinez-Garcia E, de Lorenzo V. Pseudomonas putida as a synthetic biology chassis and a metabolic engineering platform. Curr Opin Biotechnol. 2024;85:103025. Epub 20231207. doi: 10.1016/j.copbio.2023.103025. PubMed PMID: 38061264.

39. Gao T, Guo J, Niu W. Genetic Code Expansion in Pseudomonas putida KT2440. Methods Mol Biol. 2024;2760:209-17. doi: 10.1007/978-1-0716-3658-9_13. PubMed PMID: 38468091.

40. Stork DA, Squyres GR, Kuru E, Gromek KA, Rittichier J, Jog A, Burton BM, Church GM, Garner EC, Kunjapur AM. Designing efficient genetic code expansion in Bacillus subtilis

to gain biological insights. Nat Commun. 2021;12(1):5429. Epub 20210914. doi: 10.1038/s41467-021-25691-4. PubMed PMID: 34521822; PMCID: PMC8440579.

41. He X, Gao T, Chen Y, Liu K, Guo J, Niu W. Genetic Code Expansion in Pseudomonas putida KT2440. ACS Synth Biol. 2022;11(11):3724-32. Epub 20221026. doi: 10.1021/acssynbio.2c00325. PubMed PMID: 36287825; PMCID: PMC10656745.

42. Ozer E, Yaniv K, Chetrit E, Boyarski A, Meijler MM, Berkovich R, Kushmaro A, Alfonta L. An inside look at a biofilm: Pseudomonas aeruginosa flagella biotracking. Sci Adv. 2021;7(24). Epub 20210611. doi: 10.1126/sciadv.abg8581. PubMed PMID: 34117070; PMCID: PMC8195488.

43. Zhou W, Wesalo JS, Liu J, Deiters A. Genetic code expansion in mammalian cells: A plasmid system comparison. Bioorg Med Chem. 2020;28(24):115772. Epub 20200919. doi: 10.1016/j.bmc.2020.115772. PubMed PMID: 33069552; PMCID: PMC7961839.

44. Gan R, Perez JG, Carlson ED, Ntai I, Isaacs FJ, Kelleher NL, Jewett MC. Translation system engineering in Escherichia coli enhances non-canonical amino acid incorporation into proteins. Biotechnol Bioeng. 2017;114(5):1074-86. Epub 20170202. doi: 10.1002/bit.26239. PubMed PMID: 27987323; PMCID: PMC5360495.

45. de Boer HA, Comstock LJ, Vasser M. The tac promoter: a functional hybrid derived from the trp and lac promoters. Proc Natl Acad Sci U S A. 1983;80(1):21-5. doi: 10.1073/pnas.80.1.21. PubMed PMID: 6337371; PMCID: PMC393301.

46. Bailey MJ, Lilley AK, Thompson IP, Rainey PB, Ellis RJ. Site directed chromosomal marking of a fluorescent pseudomonad isolated from the phytosphere of sugar beet; stability and potential for marker gene transfer. Mol Ecol. 1995;4(6):755-63. doi: 10.1111/j.1365-294x.1995.tb00276.x. PubMed PMID: 8564013.

47. Wilson A, Fossen EV, Shrestha R, Trotter V, Poirier B, Frank A, Nelson W, Kim Y-M, Deutschbauer A, Egbert R, Elmore JR. A novel phenylpropanoid methyl esterase enables catabolism of aromatic compounds that inhibit biological nitrification. bioRxiv. 2023:2023.06.02.543320. doi: 10.1101/2023.06.02.543320.

48. Seto M, Kimbara K, Shimura M, Hatta T, Fukuda M, Yano K. A Novel Transformation of Polychlorinated Biphenyls by Rhodococcus sp. Strain RHA1. Appl Environ Microbiol. 1995;61(9):3353-8. doi: 10.1128/aem.61.9.3353-3358.1995. PubMed PMID: 16535122; PMCID: PMC1388576.

49. Van der Geize R, Yam K, Heuser T, Wilbrink MH, Hara H, Anderton MC, Sim E, Dijkhuizen L, Davies JE, Mohn WW, Eltis LD. A gene cluster encoding cholesterol catabolism in a soil actinomycete provides insight into Mycobacterium tuberculosis survival in macrophages. Proc Natl Acad Sci U S A. 2007;104(6):1947-52. Epub 20070130. doi: 10.1073/pnas.0605728104. PubMed PMID: 17264217; PMCID: PMC1794314.

50. Martinkova L, Uhnakova B, Patek M, Nesvera J, Kren V. Biodegradation potential of the genus Rhodococcus. Environ Int. 2009;35(1):162-77. Epub 20080911. doi: 10.1016/j.envint.2008.07.018. PubMed PMID: 18789530.

51. Spence EM, Calvo-Bado L, Mines P, Bugg TDH. Metabolic engineering of Rhodococcus jostii RHA1 for production of pyridine-dicarboxylic acids from lignin. Microb Cell Fact.

2021;20(1):15. Epub 20210119. doi: 10.1186/s12934-020-01504-z. PubMed PMID: 33468127; PMCID: PMC7814577.

52. Dunkelmann DL, Chin JW. Engineering Pyrrolysine Systems for Genetic Code Expansion and Reprogramming. Chem Rev. 2024;124(19):11008-62. Epub 20240905. doi: 10.1021/acs.chemrev.4c00243. PubMed PMID: 39235427; PMCID: PMC11467909.

53. Best MD. Click chemistry and bioorthogonal reactions: unprecedented selectivity in the labeling of biological molecules. Biochemistry. 2009;48(28):6571-84. doi: 10.1021/bi9007726. PubMed PMID: 19485420.

54. Yanagisawa T, Ishii R, Fukunaga R, Kobayashi T, Sakamoto K, Yokoyama S. Multistep engineering of pyrrolysyl-tRNA synthetase to genetically encode N(epsilon)-(o-azidobenzyloxycarbonyl) lysine for site-specific protein modification. Chem Biol. 2008;15(11):1187-97. doi: 10.1016/j.chembiol.2008.10.004. PubMed PMID: 19022179.

55. Bryson DI, Fan C, Guo LT, Miller C, Soll D, Liu DR. Continuous directed evolution of aminoacyl-tRNA synthetases. Nat Chem Biol. 2017;13(12):1253-60. Epub 20171016. doi: 10.1038/nchembio.2474. PubMed PMID: 29035361; PMCID: PMC5724969.

56. da Cruz Nizer WS, Inkovskiy V, Versey Z, Strempel N, Cassol E, Overhage J. Oxidative Stress Response in Pseudomonas aeruginosa. Pathogens. 2021;10(9). Epub 20210914. doi: 10.3390/pathogens10091187. PubMed PMID: 34578219; PMCID: PMC8466533.

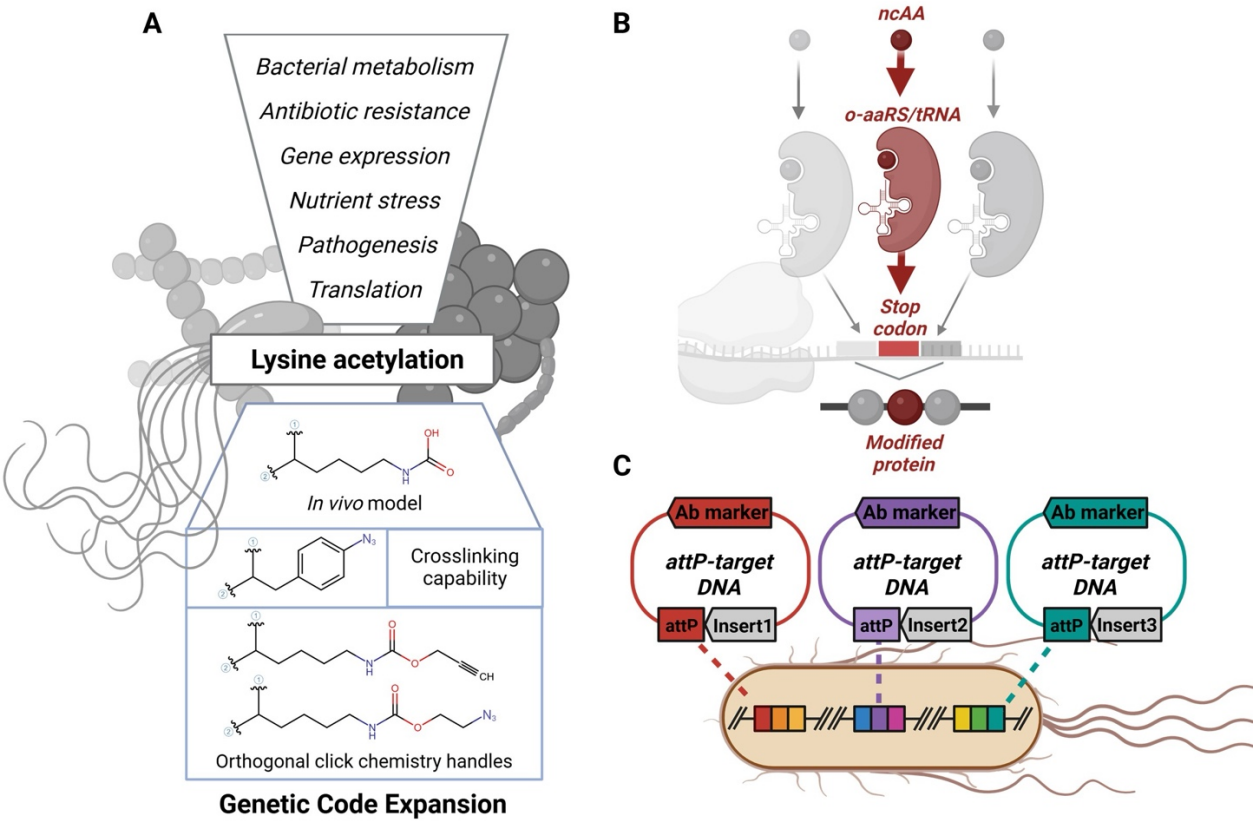

Figure 1. A. Overview of lysine acetylation in diverse bacteria. Included are the chemical structures of ncAA employed in acetyl lysine interrogation. **B.** Overview of Genetic Code Expansion (GCE). Elements in red represent engineered translational components that act orthogonally to endogenous translation to produce site-specifically modified protein. **C.** Overview of Serine-recombinase Assisted Genome Engineering (SAGE) where serine-recombinases encoded on non-replicating plasmids facilitate the insertion of *attP*-containing target plasmids into cognate *attB*-sequences that have been installed into the host chromosome.

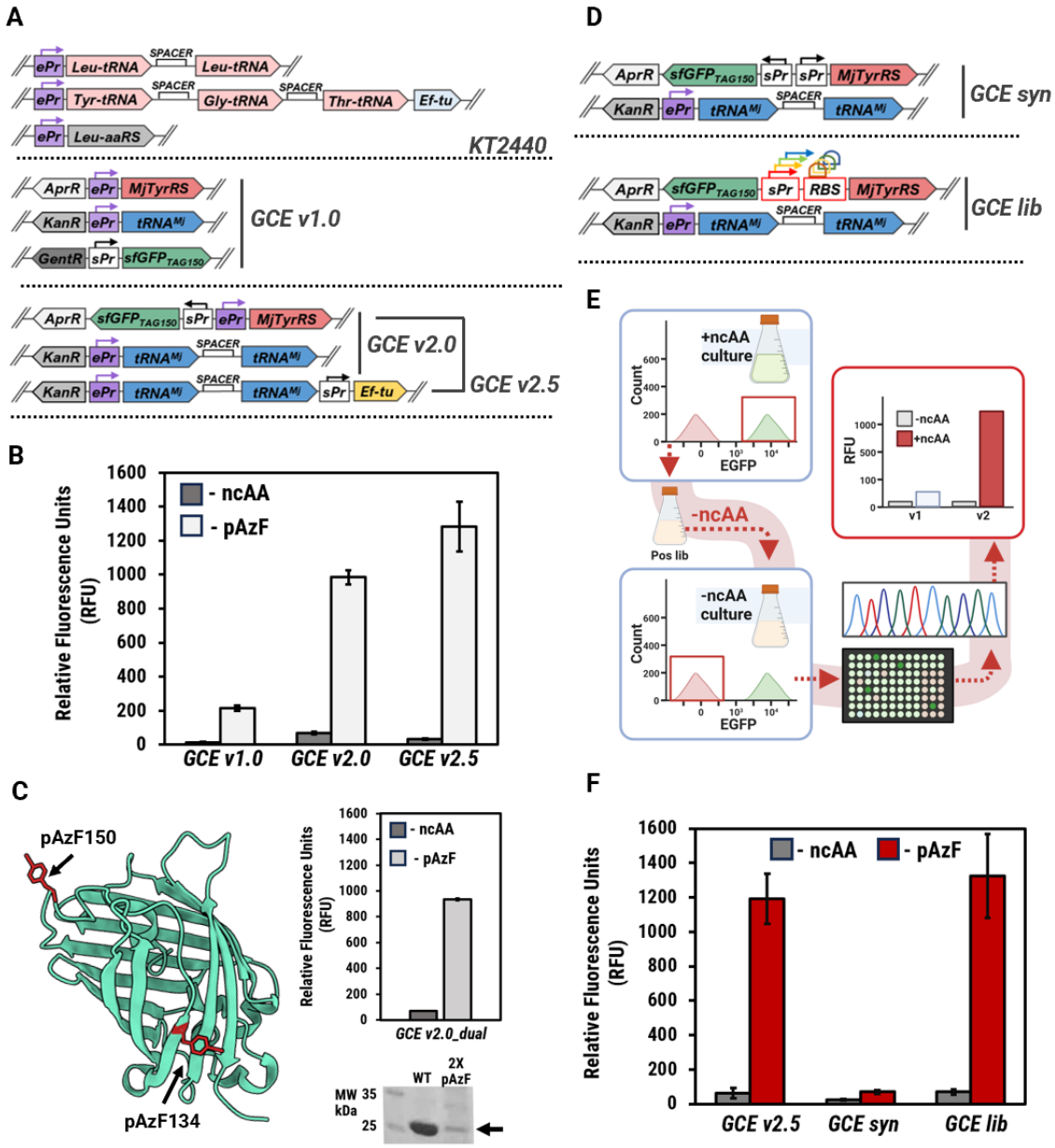

Figure 2. A. Overview of endogenous and initial GCE translational systems utilized in this work. **B.** GCE efficiency assays for KT2440 GCE-SAGE systems from four biologically independent cultures. The GCE system used is indicated below each column set on the *x*-axis. The ncAA condition for each system is disclosed in a legend in the upper left of the figure. **C.** Overview of dual incorporation system. Structure of sfGFP is indicated on the left with each site indicated in red. GCE incorporation efficiency for the dual incorporation system is shown on the right from large scale expression cultures of KT2440. SDS-PAGE of 2X pAzF shown side-by-side with WT GFP, protein band of interest is indicated by arrow. **D.** Overview of GCE synthetic translational systems and GCE library scheme. **E.** Scheme of FACS-based library selection for promoter optimization. After transformation into KT2440, the promoter library is cultured in the presence of ncAA to elicit a fluorescent signal. Fluorescent events are sorted via FACS and cultured in the absence of ncAA. Low fluorescent events are then plate sorted for sequencing and final validation. **F**. GCE efficiency assays for KT2440 GCE synthetic translational system and optimized GCE library system from four biologically independent cultures. The ncAA condition for each system is disclosed in a legend at the top of the figure.

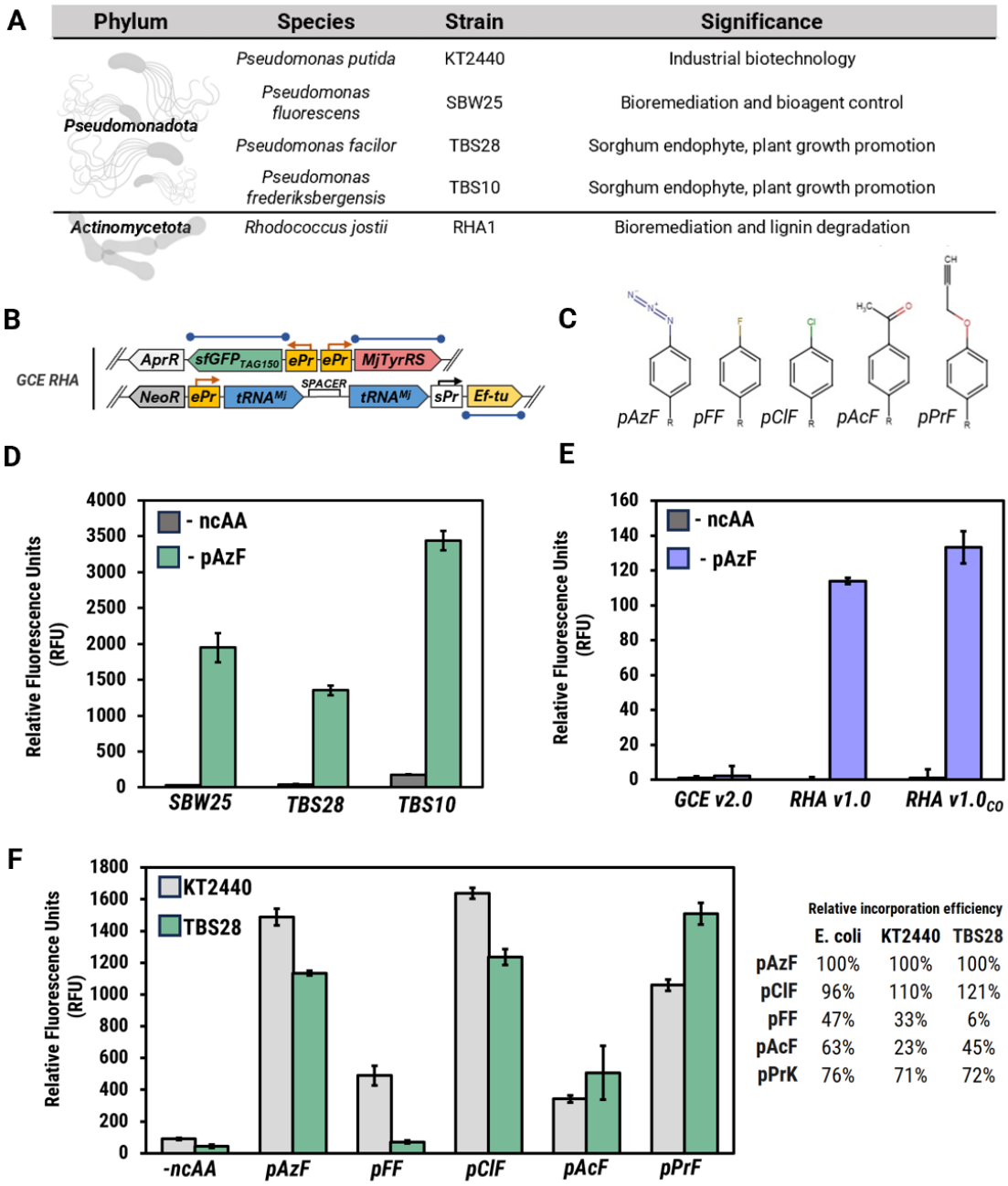

Figure 3. A. Overview of bacterial species used in this study**. B.** Overview of RHA1 GCE translational systems. **C.** Structures of ncAAs screened in KT2440 and TBS28 strains. **D.** GCE efficiency assays for GCE v2.0 in three pseudomonads. The pseudomonad used is indicated below each column set on the *x*-axis. The ncAA condition for each system is disclosed in a legend in the upper left of the figure. **E.** GCE efficiency assays for GCE v2.0 vs GCE RHA in RHA1. The GCE system used is indicated below each column set on the *x*-axis. The ncAA condition for each system is disclosed in a legend in the upper left of the figure. **F.** ncAA incorporation efficiency assay for KT2440 and TBS28 with GCE v2.0. The ncAA system used is indicated below each column set on the *x*-axis. The strain (either KT2440 or TBS28) disclosed in a legend in the upper left of the figure. The incorporation efficiency of each ncAA relative to pAzF are shown for E. coli, KT2440 and TBS28.

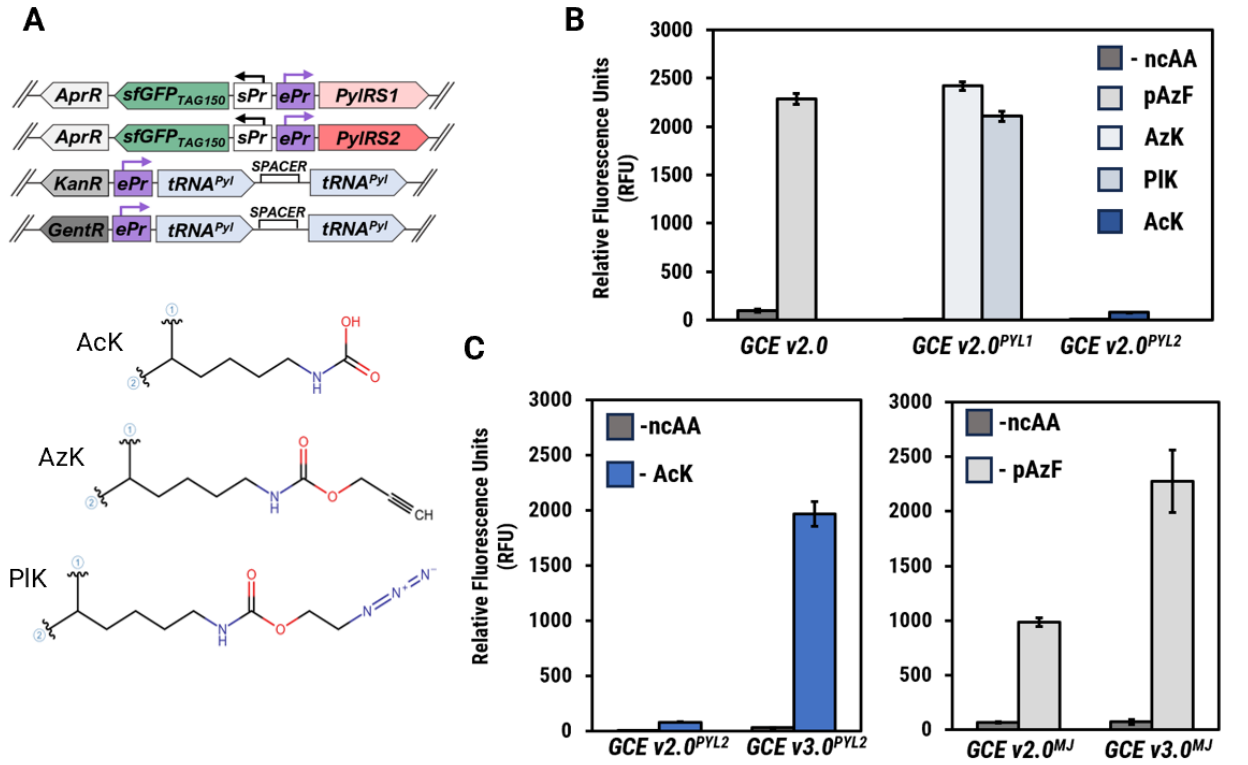

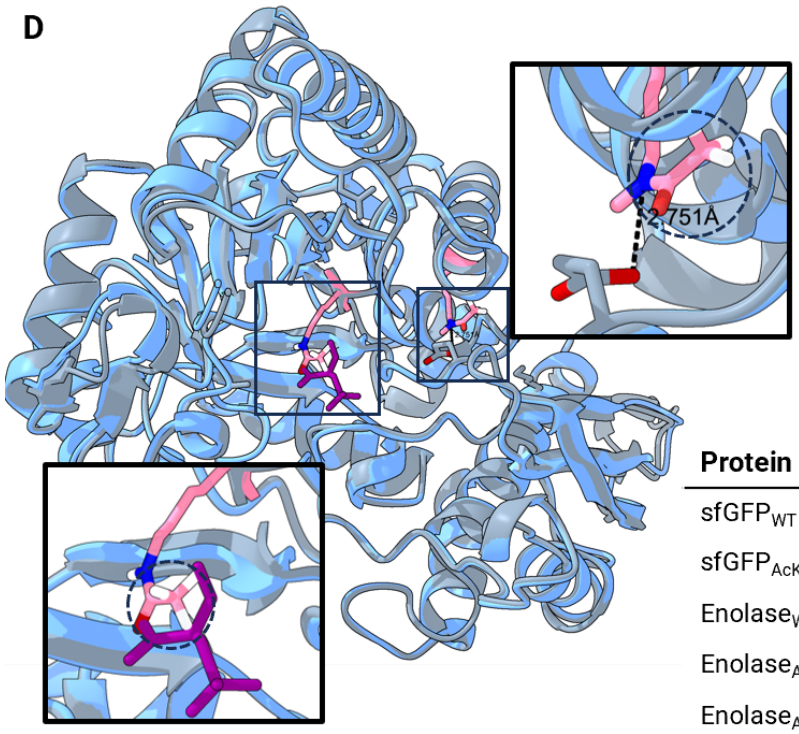

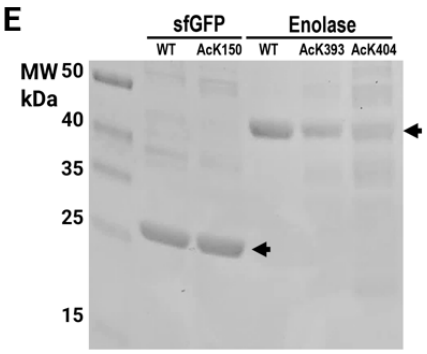

Protein	MW_{Calc} (Da)	MW_{Obs} (Da)
$sfGFP_{WT}$	27813.89	27812.0020
$sfGFP_{AcK150}$	27870.07	27868.0020
$Enolase_{WT}$	46326.37	46326.0039
$Enolase_{AcK392}$	46368.37	46368.0039
$Enolase_{AcK404}$	46368.37	46369.0039

Figure 4. A . Overview of GCE systems with Pyl components. Structures of ncAAs incorporated with Pyl components are shown underneath**. B.** GCE efficiency assays with Pyl systems in KT2440. The GCE system used is indicated below each column set on the *x*-axis. The ncAA condition for each system is disclosed in a legend in the right left of the figure. **C.** GCE efficiency assays comparing GCE v2.0 with GCE v3.0. Pyl system and *Mj* systems in KT2440 are compared in left panels and right panels respectively. The GCE system used is indicated below each column set on the *x*-axis. The ncAA condition for each system is disclosed in a legend in the top left of the figure. **D.** Structure of enolase with acetyl lysines and bound substrate. Alpha fold generated structure of KT2440 enolase with acetylations modeled relevant lysine residues (blue ribbon structure) overlaid on PDB structure of enolase from E. coli (gray ribbon structure) with bound substrate 2PGA (purple molecule). Acetyl grounds are circled. **E.** SDS-PAGE of acetylated proteins, purified from KT2440. Arrows indicate the MW for each set of purified proteins. **F.** Observed intact masses of purified acetylated proteins with their respective calculated masse**s.**

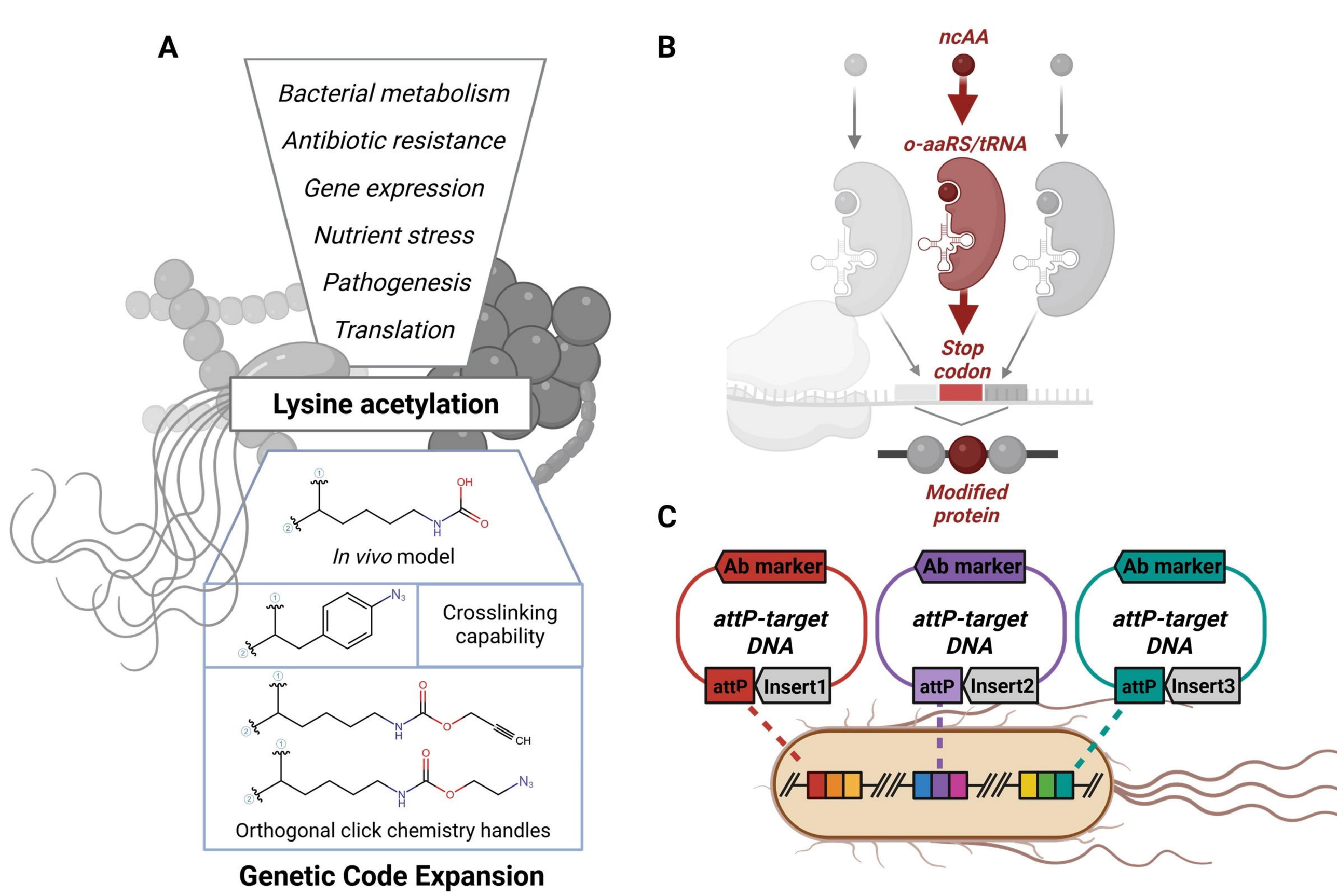
A
Bacterial metabolism
Antibiotic resistance
Gene expression
Nutrient stress
Pathogenesis
Translation
Lysine acetylation
In vivo model
Crosslinking capability
Orthogonal click chemistry handles
Genetic Code Expansion
B
ncAA
o-aaRS/tRNA
Stop codon
Modified protein
C
Ab marker
attP-target DNA
attP
Insert1
Ab marker
attP-target DNA
attP
Insert2
Ab marker
attP-target DNA
attP
Insert3

A

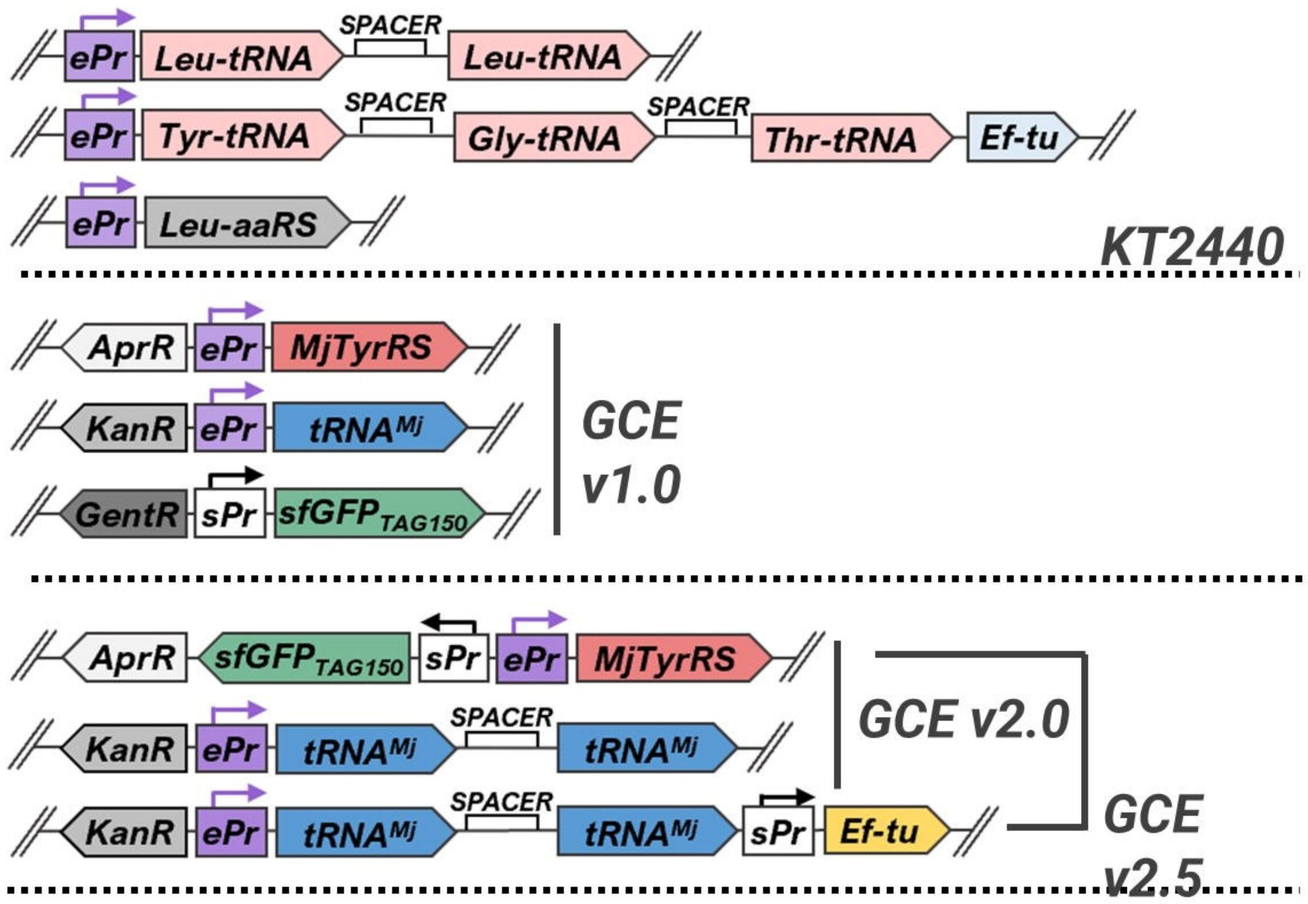
ePr
Leu-tRNA
SPACER
Leu-tRNA
ePr
Tyr-tRNA
SPACER
Gly-tRNA
SPACER
Thr-tRNA
Ef-tu
ePr
Leu-aaRS
KT2440
AprR
ePr
MjTyrRS
KanR
ePr
tRNAMj
GentR
sPr
sfGFPTAG150
GCE v1.0
AprR
sfGFPTAG150
sPr
ePr
MjTyrRS
KanR
ePr
tRNAMj
SPACER
tRNAMj
KanR
ePr
tRNAMj
SPACER
tRNAMj
sPr
Ef-tu
GCE v2.0
GCE v2.5

B

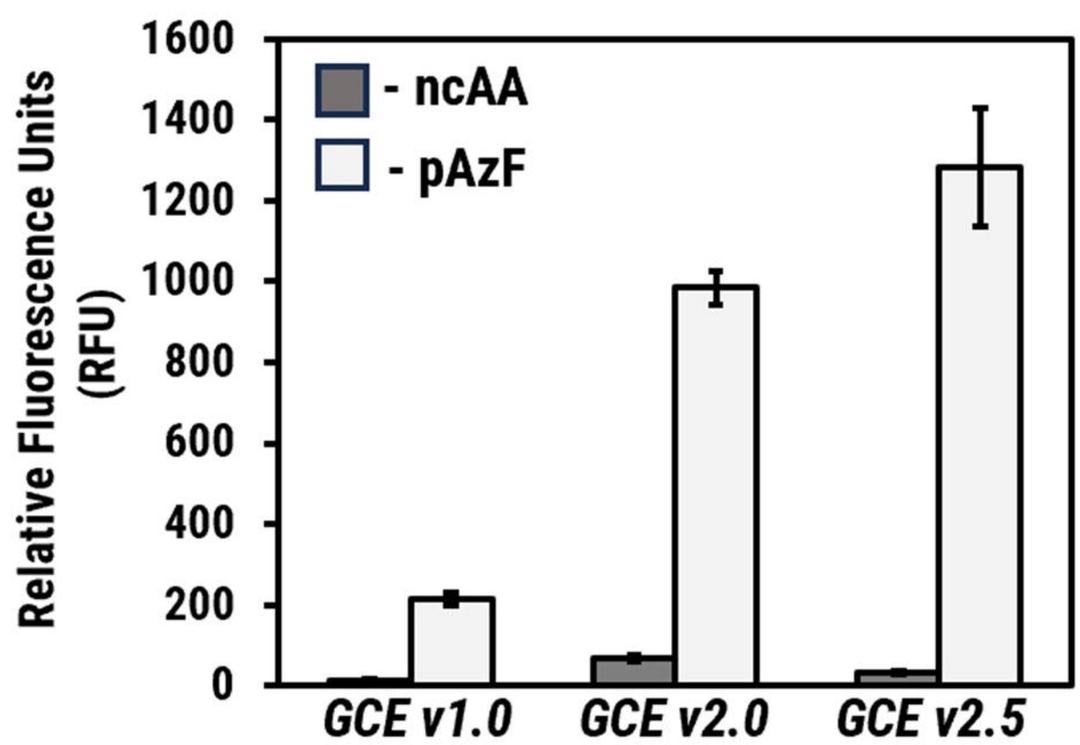
Relative Fluorescence Units (RFU)
1600
1400
1200
1000
800
600
400
200
0
- ncAA
- pAzF
GCE v1.0
GCE v2.0
GCE v2.5

C

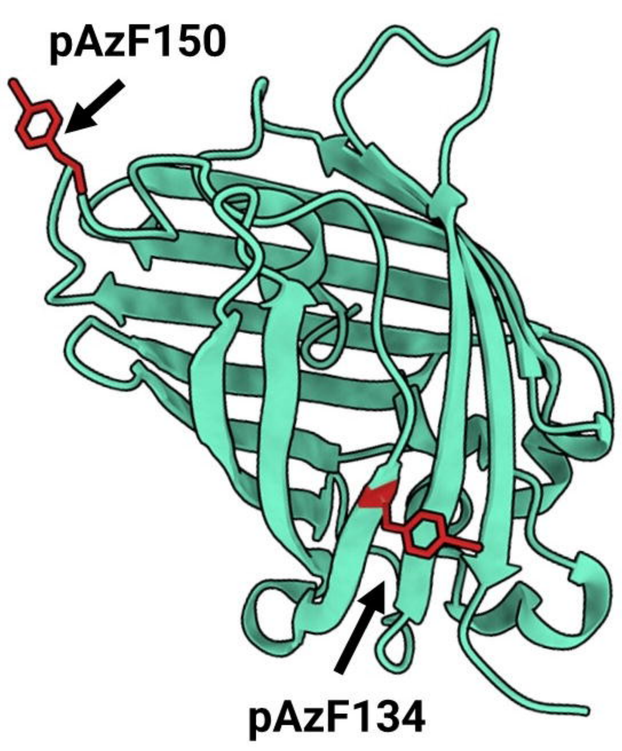
pAzF150
pAzF134

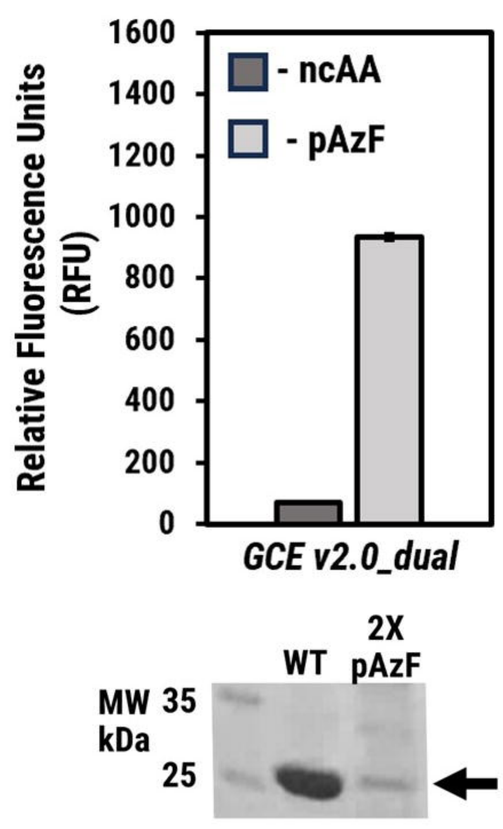
Relative Fluorescence Units (RFU)
1600
1400
1200
1000
800
600
400
200
0
- ncAA
- pAzF
GCE v2.0_dual
WT
2X pAzF
MW kDa
35
25

D

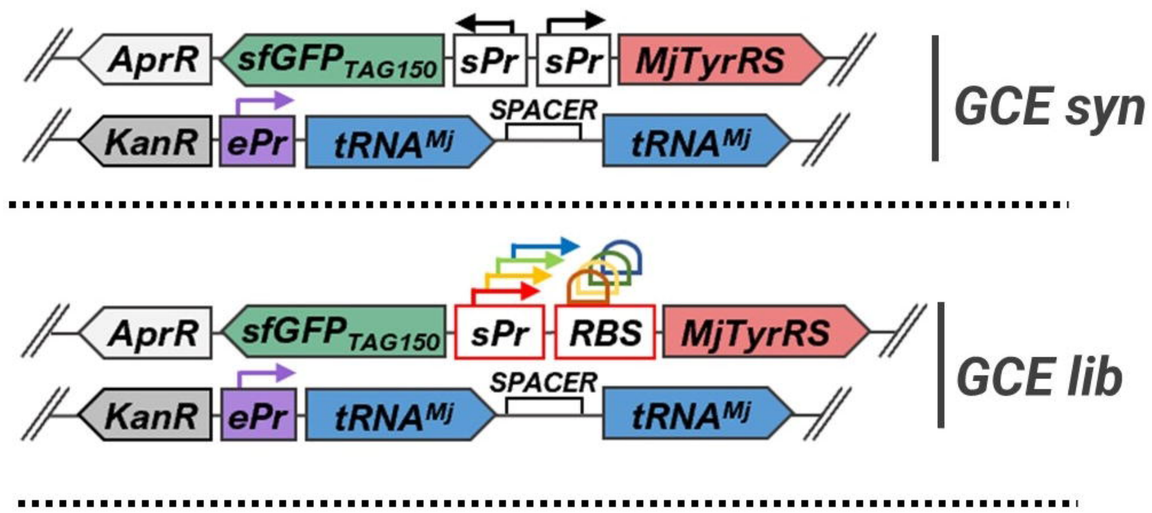
AprR
sfGFPTAG150
sPr
sPr
MjTyrRS
KanR
ePr
tRNAMj
SPACER
tRNAMj
GCE syn
AprR
sfGFPTAG150
sPr
RBS
MjTyrRS
KanR
ePr
tRNAMj
SPACER
tRNAMj
GCE lib

E

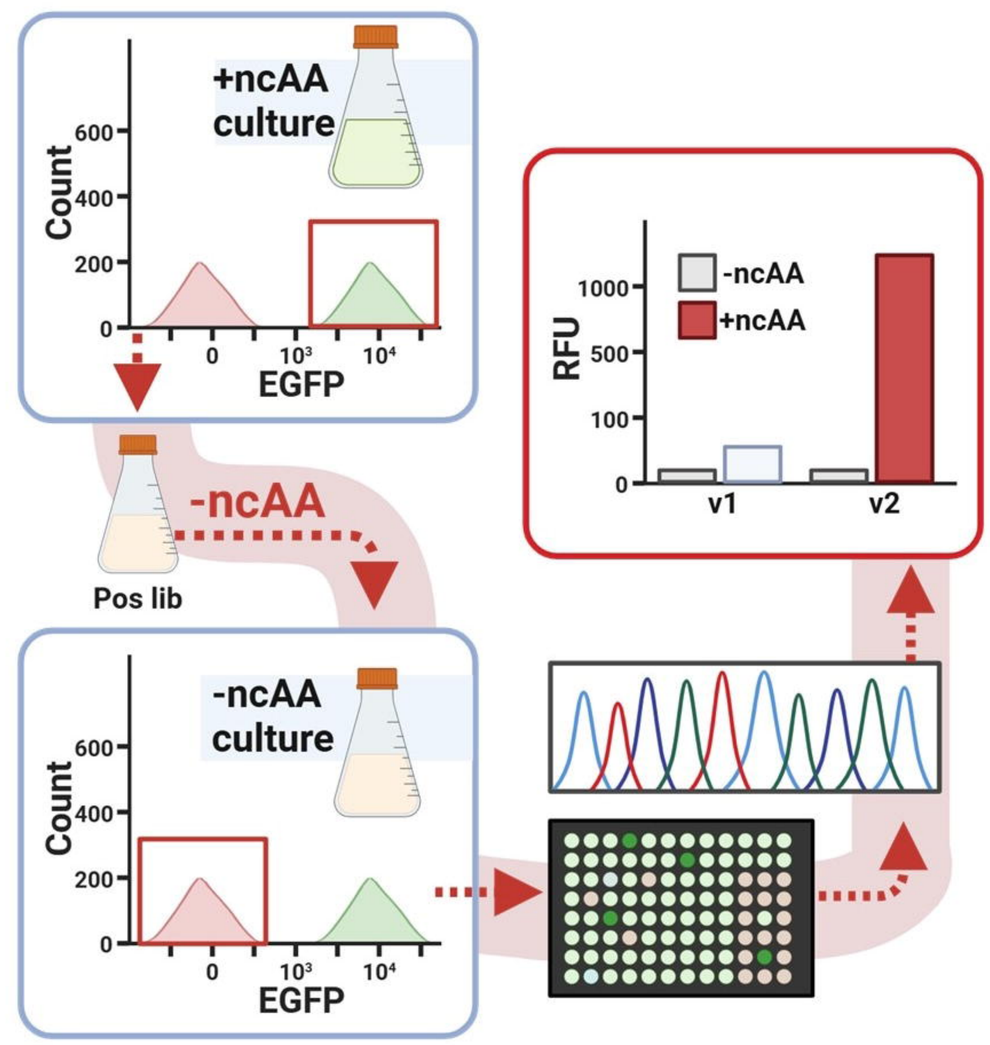
+ncAA culture
Count
600
400
200
0
0
10³
10⁴
EGFP
-ncAA
Pos lib
-ncAA culture
Count
600
400
200
0
0
10³
10⁴
EGFP
RFU
1000
500
100
0
-ncAA
+ncAA
v1
v2

F

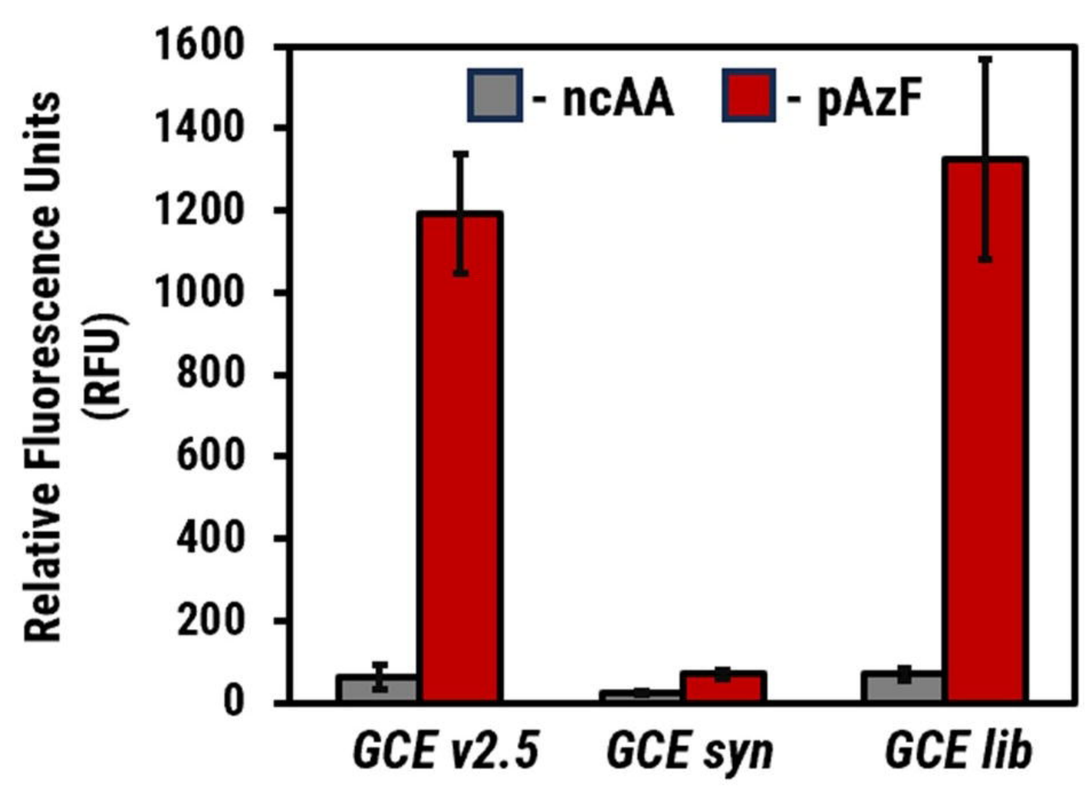
Relative Fluorescence Units (RFU)
1600
1400
1200
1000
800
600
400
200
0
- ncAA
- pAzF
GCE v2.5
GCE syn
GCE lib

A

Phylum	Species	Strain	Significance
Pseudomonadota	*Pseudomonas putida*	KT2440	Industrial biotechnology
	Pseudomonas fluorescens	SBW25	Bioremediation and bioagent control
	Pseudomonas facilor	TBS28	Sorghum endophyte, plant growth promotion
	Pseudomonas frederiksbergensis	TBS10	Sorghum endophyte, plant growth promotion
Actinomycetota	*Rhodococcus jostii*	RHA1	Bioremediation and lignin degradation

B

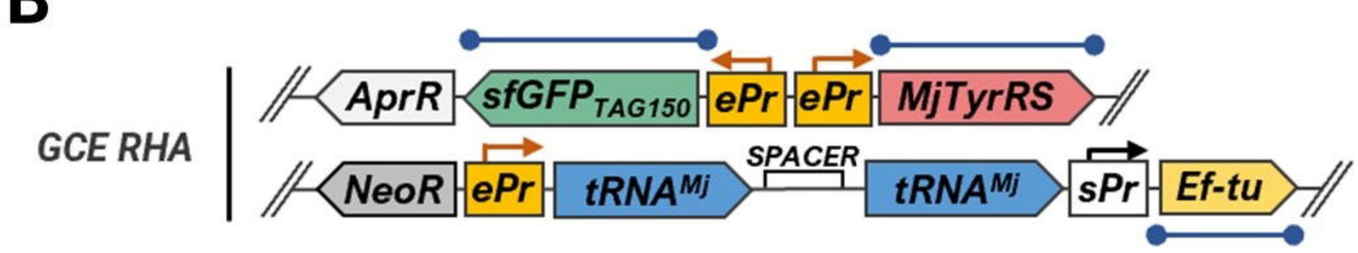

C

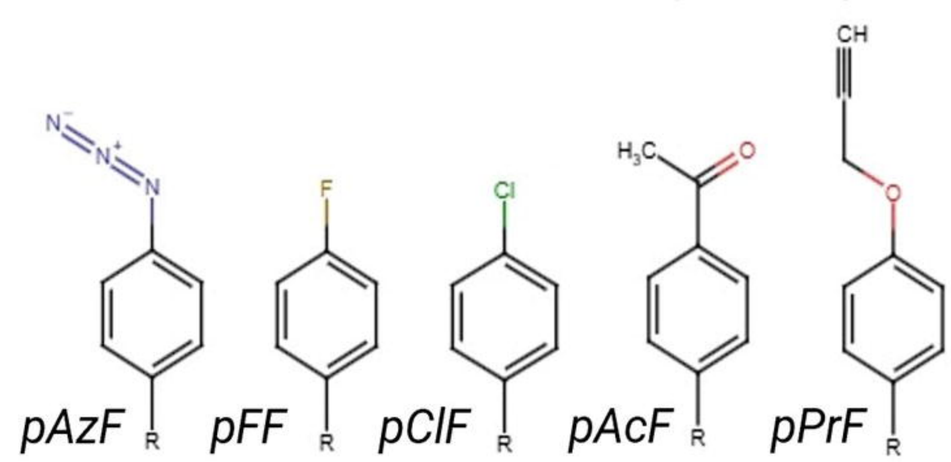

D

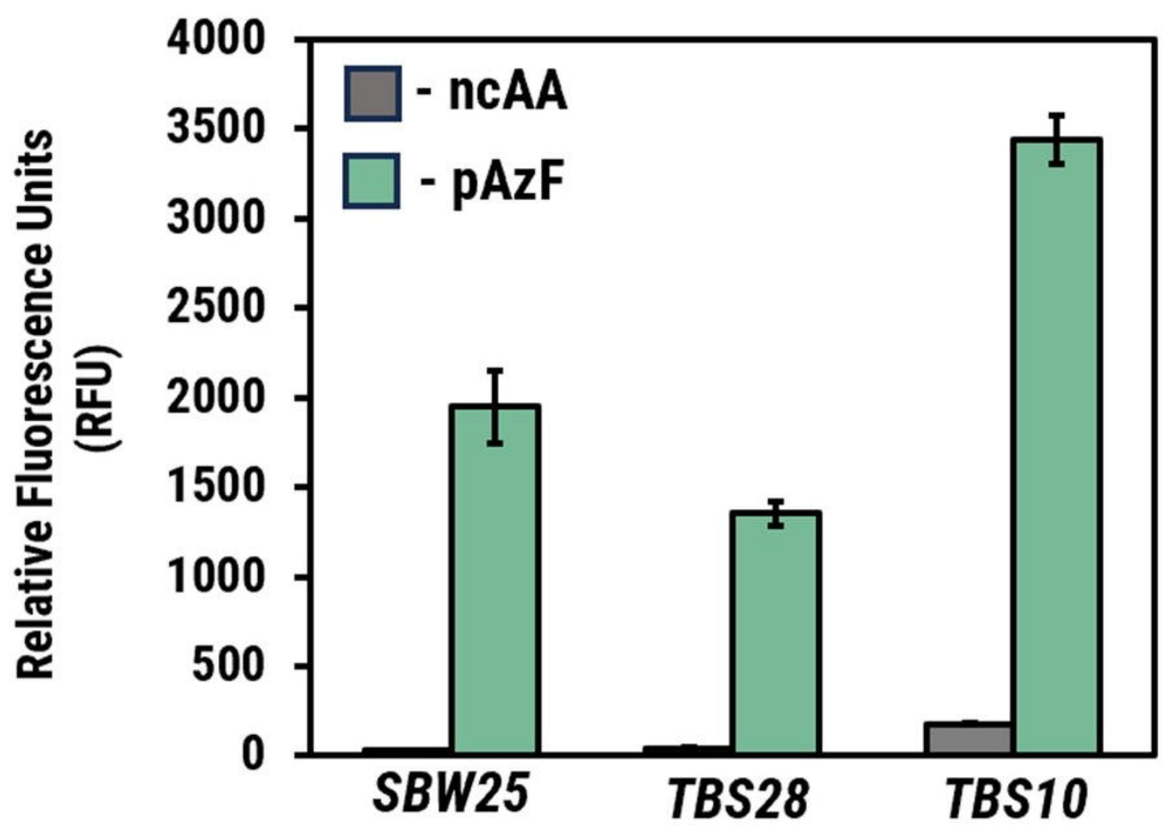

E

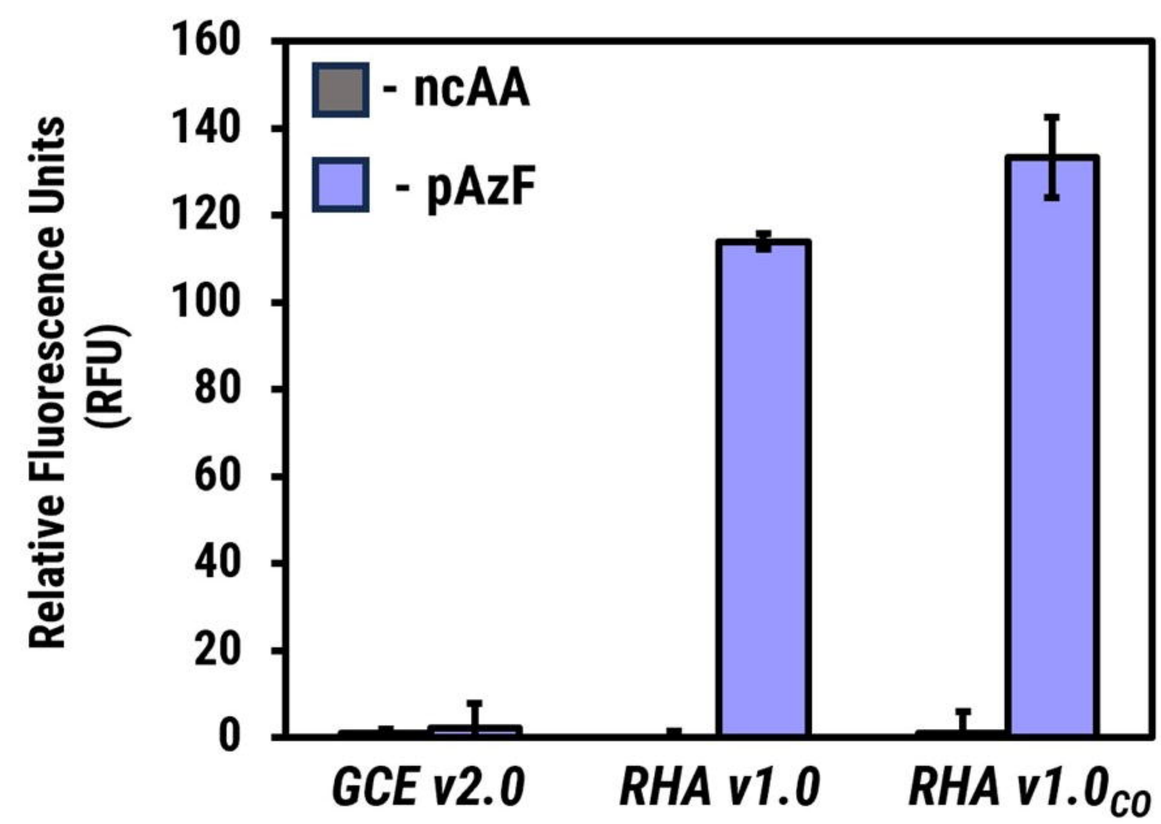

F

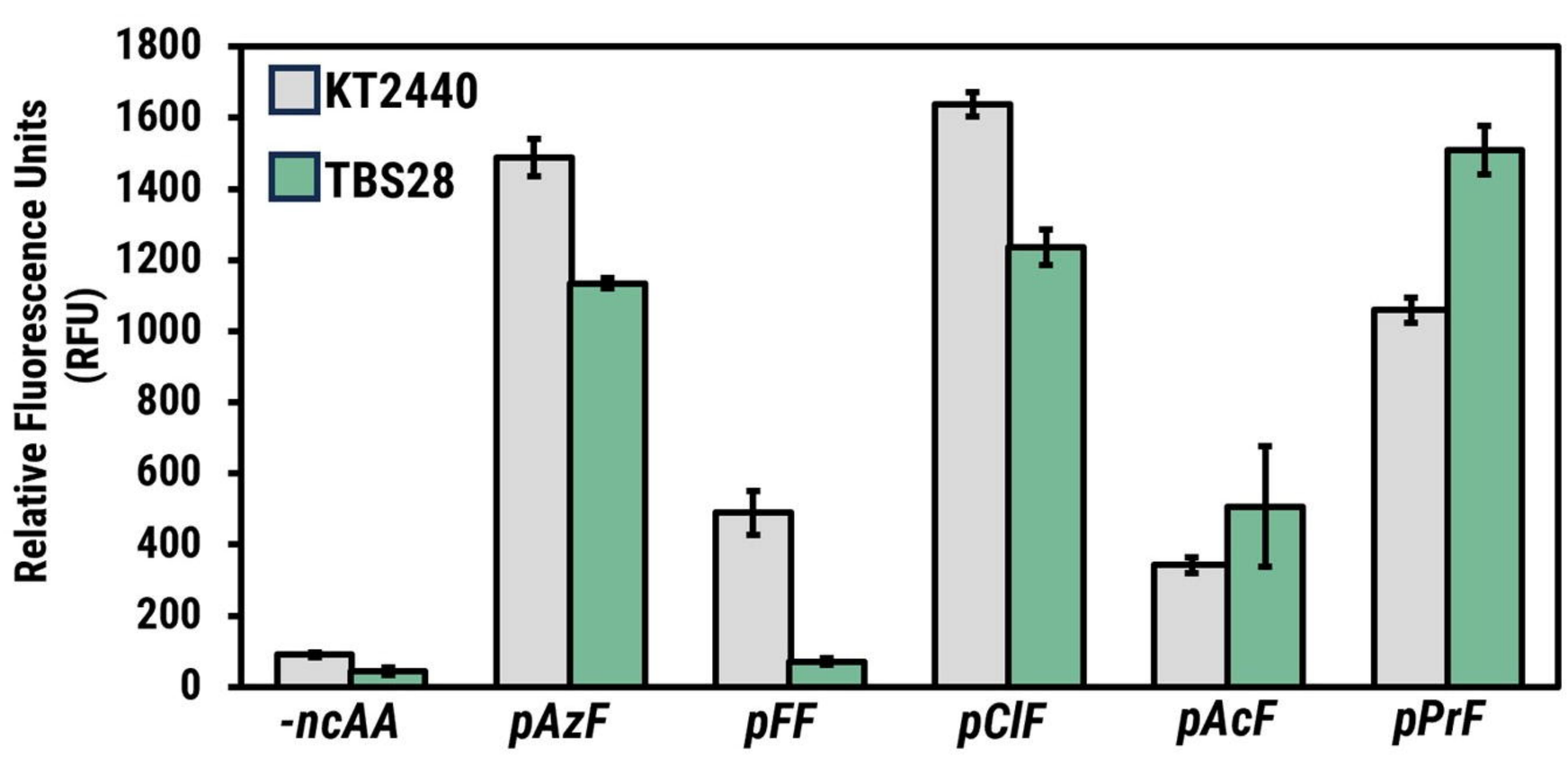

Relative incorporation efficiency

	E. coli	KT2440	TBS28
pAzF	100%	100%	100%
pClF	96%	110%	121%
pFF	47%	33%	6%
pAcF	63%	23%	45%
pPrK	76%	71%	72%

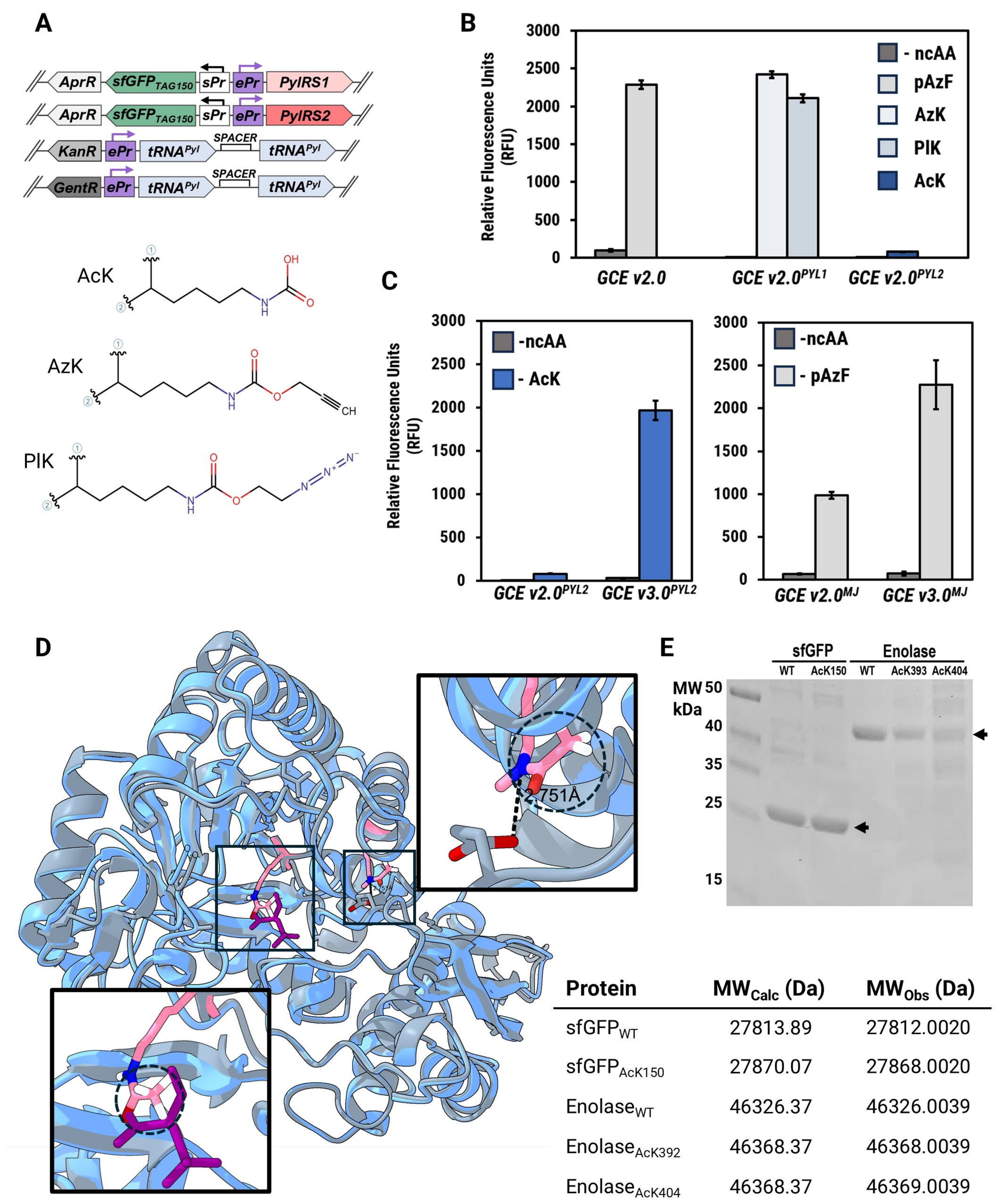

Protein	MW_{Calc} (Da)	MW_{Obs} (Da)
$sfGFP_{WT}$	27813.89	27812.0020
$sfGFP_{AcK150}$	27870.07	27868.0020
$Enolase_{WT}$	46326.37	46326.0039
$Enolase_{AcK392}$	46368.37	46368.0039
$Enolase_{AcK404}$	46368.37	46369.0039